MIDDLE EAST TECHNICAL UNIVERSITY

EARTHQUAKE ENGINEERING RESEARCH CENTER

# PERFORMANCE COMPARISON OF HIGH-DAMPING RUBBER ISOLATORS AND FRICTION PENDULUM ISOLATORS WITH DIFFERENT MODELLING APPROACHES

List of Collaborators

| Sismolab-METU | Bridgestone Corporation | Istanbul Technical University |
|---|---|---|
| Eser Çabuk | Nobuo Murota | |
| Uğurhan Akyüz | Shigenobu Suzuki | Fatih Sütçü |
| Ahmet Yakut | Takahiro Mori | |


REPORT NO: METU/EERC 2020-02

JUNE 2020

## ACKNOWLEDGEMENTS

This research was jointly supported by SISMOLAB and BRIDGESTONE CORPORATION. The authors would like to express the greatest appreciation to all the staff involved in this project for their generous cooperation.

## ABSTRACT

In Turkey, seismic isolation applications have become one of the most widely used methods to mitigate adverse effects of earthquakes on both structural and non-structural components among important buildings, especially after the regulations of Ministry of Health regarding the hospitals located in high seismic zones. Lead rubber bearings and friction pendulum systems have gained popularity and are applied among variety of structures. However, high damping rubber bearings (HDRB), have not been widely used in these applications attributable to the lack of knowledge and technology for advanced rubber material. In order clarify the design, analysis steps, seismic performance and applicability of HDRB isolators a seismically isolated hospital, which was built with friction pendulum system (FPS) based on Turkish Building Seismic Code 2018, is evaluated by numerical analysis. The 10-story hospital building model was modelled by ETABS, and HDRB design for a target performance has been conducted. The building model with both HDRB and FPS designs were analyzed under different earthquake levels specified in the code. Also, variety of mathematical link models, provided in ETABS, were used in the analyses stage to investigate the effect of the modeling difference on the results. Nonlinear time history and modal superposition analyses were conducted, and results were compared in terms of performance parameters. Results show that there is significant influence of isolator modeling approach on the seismic response. Comments were also made according to the new Turkish Building Seismic Code.

# Table of Contents

## List of Figures

## List of Tables

# 1 INTRODUCTION

## 1.1 Development of Seismic Isolation Applications in Turkey

Seismic isolation applications are a preferable option not only for reducing the earthquake effects on structures and being able to use them immediately after earthquakes but also preventing the damage on non-structural components. It has been widely used in developed countries with high seismicity.

In Turkey, seismic isolation applications are recently becoming more popular among important structures such as hospitals, data centers, and bridges [1], especially after the regulations of the Ministry of Health (MoH) in 2013 that makes it mandatory to use seismic isolation in governmental hospitals having a bed capacity of more than 100 and located in high seismic regions. The MoH regulations were updated in 2018, and it includes requirements and specifications on the planning, seismic design, analysis, testing, application, and maintenance stages of isolation units.

Rubber bearings have been extensively used on buildings and bridges as seismic isolation devices [2]. Moreover, lead core rubber bearings (LRB) [3] and friction pendulum systems (FPS) [4] are the most widely used isolation systems among hospitals, data centers, and bridges in the world. Although high damping rubber bearing (HDRB) [5] is another type of commonly used isolation system in the globe, it is not widely used among seismically isolated projects in Turkey, despite its high energy absorption capacity. This may be attributed to the lack of knowledge on the design, analysis and the technology. Gaining knowledge and experience on the theory, modeling and application of such systems are important as improper design and lack of knowledge may result in fatal damages on structures, casualties and significant economic loss.

## 1.2 High-damping Rubber Bearing

HDRB is a type of seismic rubber bearings that is composed of laminated thin rubber layers and reinforcing steel plates. HDRB uses rubber material which has energy dissipation characteristics and provides damping properties as well as the elasticity of rubber for seismic isolation similar to LRB or FPS. The rubber material used for HDRB is a specially designed compound that generates internal friction between polymer and filler, such as carbon, during deformation, which enables energy dissipation. The oval rounded-shape hysteresis curve is one of the typical characteristics of

HDRB, which generally gives significant merit in reducing high-mode vibration of superstructures, especially in large deformation states. On the other hand, the damping mechanism by the polymer-filler structure results with a relatively high nonlinearity in its stress-strain relationship. Therefore, the difficulty in numerical representation of shear force-displacement has generally been a challenge for structural engineers to apply the HDRB in seismic isolation systems. Recently, a new numerical model that accurately represents the nonlinear restoring force characteristics of HDRB2 has been developed [6, 7, 8] and proven to be applicable in commercial structure-design software, such as ETABS and SAP2000 [9]. This simplifies the modelling of HDRBs in practical use for structural engineers.

### 1.3 Friction Pendulum Systems

Sliding systems have been implemented first in bridges using Teflon material to accommodate the relatively low displacements caused by the temperature changes, shrinkage, and creep behavior of the concrete [16]. At the beginning, these systems did not provide any re-centering capability because of the flat surface shape. Over the years, many types of sliding isolators have been developed with different materials and various types of curved surfaces and have been used not only in bridges but also in nuclear power plants, buildings, and other type of structures.

Friction pendulum isolators mainly work with the principle of a pendulum. They consist of sliding steel surfaces and a sliding material. FPS allows the building to undergo horizontal displacements providing a specified required period. The gravity acts as a re-centering force and brings the building back to its original position. The performance is mainly affected by two design parameters, radius of curvature ($R$) and coefficient of friction ($\mu$). Re-centering effects are produced by vertical load ($P$) on the isolator and radius of curvature (R), and energy dissipation is obtained by the dynamic friction between sliding material and curved surfaces [12].

### 1.4 Aim of the Study

In this study, the applicability of HDRB for seismic isolation of a hospital, based on Turkish Building Seismic Code [10], is evaluated by numerical simulation. Different mathematical models were used for both HDRB and FPS types. Equivalent lateral force procedure, response spectrum (modal superposition) analysis, and time-history analysis with actual seismic records scaled according to the target spectra is conducted and response characteristics of the superstructure, such as response acceleration, story drift and behavior of isolation interface are investigated. The results are compared to that of double curved surface FPS and special attention is paid to the difference in the behavior of superstructures and isolation system. Furthermore, hysteretic behavior of isolators under each mathematical model are also investigated and differences in the results are highlighted in terms of axial load behavior, hysteretic stability, secondary stiffness, and energy dissipation.

# 2 MODELLING

## 2.1 Building Model

The building is one of the ten-story T-shaped blocks of a seismically isolated reinforced concrete hospital building. Shear walls and frame elements constitute the structural system and friction pendulum isolators (total 118 isolators) have been used in the design and construction of the building. The plan geometry of the building is 115 m in horizontal and 75 m in the vertical direction and the total height is 40 m. Column dimensions are 1250x1250 mm under the isolation level, 900x900 mm on the first floor above the isolation level and 800x800 mm in upper stories. Beam dimensions are varying in terms of depth and width with the maximum size of 900x600 mm. Shear wall thickness is 300 mm.

Structural analyses were conducted using a commercial structural analysis software ETABS developed by Computers and Structures Inc. The 3D-model of the building and isolation level plan are given in Figure 1. Structural weight (G+0.3Q) of the building block is 492383 kN. Rigid floor diaphragms are assigned to each floor. Fixed base period of the building has been obtained as approximately 1.65 seconds in both x and y directions. More than 85 percent modal mass participation is obtained in first ten modes for fixed base model and modal properties are shown for the first five modes in Table 1.

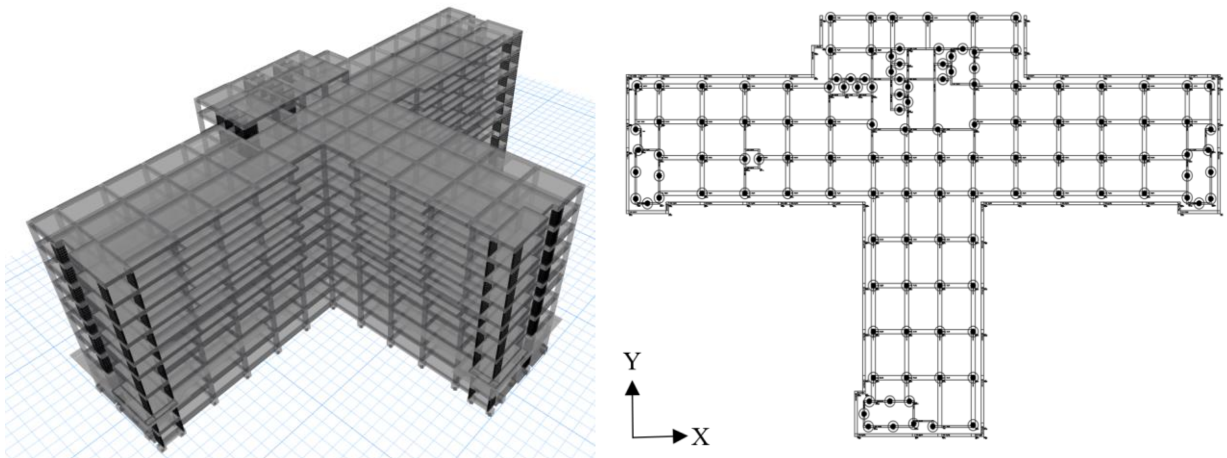


Figure 1. 3-D view of the building (left) and isolation plan (right)

Table 1. Fixed based modal properties of the building

| | | **Mass participation ratios** | |
|---|---|---|---|
| | **Period (s)** | **Mx** | **My** |
| **Mode 1** | 1.663 | 0.367 | 0.177 |
| **Mode 2** | 1.641 | 0.105 | 0.568 |
| **Mode 3** | 1.458 | 0.267 | 0.0004 |
| **Mode 4** | 0.505 | 0.012 | 0.065 |
| **Mode 5** | 0.496 | 0.041 | 0.019 |

Based on regulations specified by Turkish Ministry of Health, a site-specific response spectrum was prepared based on soil investigations on the site. Design Basis Earthquake (DBE) and Maximum Considered Earthquake (MCE) ground motion levels are considered. Based on the seismic hazard report of the site the $Vs_{30}$ value has been found as 350 m/s. The site is located nearly 25 km to an active strike-slip fault, and a magnitude of 6.9 earthquake occurred in nearest city, Burdur, in 1914.

In order to conduct nonlinear time-history analyses, seven ground motions were selected from PEER ground motion database and scaled in such a way that average of geomean scaled response spectra of ground motions will not be less than the 5% damped target design spectra as can be seen in Figure 3. The list of ground motions and their scale factors for DBE and MCE are given in Table 2. Acceleration records in two main directions for ground motions #2, #4 and #7 are shown in Appendix A. The new code requires to select eleven ground motions for nonlinear time-history analysis. However, since this is not a design project, seven ground motions, selected for the building, according to previous Turkish seismic code [9] were used.

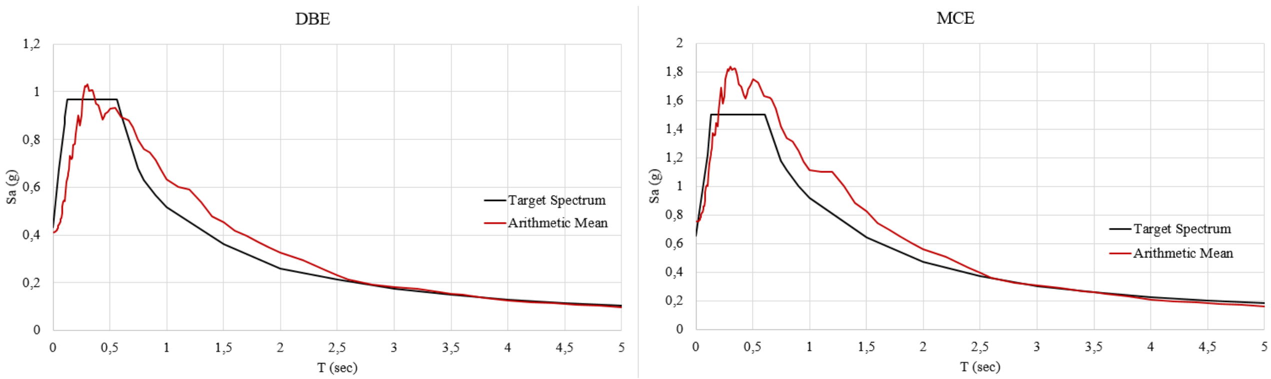


Figure 2. DBE (left) and MCE (right) level target spectra

Table 2. Selected ground motions from PEER database and scale factors

| EQ # | Record ID | Earthquake Name | Year | Station Name | Magnitude | Mechanism | Rjb (km) | Vs30 (m/sec) | Scale Factors DBE | Scale Factors MCE |
|---|---|---|---|---|---|---|---|---|---|---|
| 1 | 1605 | "Duzce_ Turkey" | 1999 | "Duzce" | 7.14 | strike slip | 0.0 | 281.86 | 0.85 | 1.21 |
| 2 | 821 | "Erzican_ Turkey" | 1992 | "Erzincan" | 6.69 | strike slip | 0.0 | 352.05 | 0.92 | 1.33 |
| 3 | 1787 | "Hector Mine" | 1999 | "Hector" | 7.13 | strike slip | 10.35 | 726.0 | 1.69 | 4.40 |
| 4 | 1116 | "Kobe_ Japan" | 1995 | "Shin-Osaka" | 6.9 | strike slip | 19.14 | 256.0 | 1.97 | 4.63 |
| 5 | 1158 | "Kocaeli_ Turkey" | 1999 | "Duzce" | 7.51 | strike slip | 13.6 | 281.86 | 1.15 | 1.87 |
| 6 | 1165 | "Kocaeli_ Turkey" | 1999 | "Izmit" | 7.51 | strike slip | 3.62 | 811.0 | 1.97 | 3.12 |
| 7 | 777 | "Loma Prieta" | 1989 | "Hollister City Hall" | 6.93 | Reverse Oblique | 27.33 | 198.77 | 0.96 | 2.28 |

## 2.2 Modeling of FPS

The hospital building has originally been isolated with the use of FPS isolators. Three types of FPS isolators were selected based on column axial compressive loads. Displacement response for DBE and MCE levels were determined as 20.9 cm and 64.3 cm, respectively. Nominal isolator properties of each type are shown in Table 3. Property modification factors $\lambda$ for upper and lower bound (UB, LB) were specified by the manufacturer as 1.56 and 0.9.

Table 3. Nominal isolator properties of friction pendulum system isolators

| **Type** | **# of iso.** | **Service Load (*G*+0.3*Q*)** | **ULS Load (1.2*G*+*Q*+*E*)** | **Friction Coefficient $\mu$** | **Radius *R*** | **$K_{eff}$-DBE** | **$K_{eff}$-MCE** |
|---|---|---|---|---|---|---|---|
| | | kN | kN | % | m | kN/m | kN/m |
| 1 | 87 | 3494 | 13181 | 5.5 | 4.5 | 1737.3 | 1160.8 |
| 2 | 25 | 6819 | 15765 | 5.5 | 4.5 | 3390.6 | 2265.4 |
| 3 | 6 | 5390 | 22670 | 5.5 | 4.5 | 2680.0 | 1790.7 |

The FPS isolators were first modeled using Friction Pendulum Isolator (FPI) link property which is implemented in ETABS [15]. The hysteretic model is first proposed in [17] and [18] and recommended in [16] for base isolation applications. Furthermore, the pendulum behavior is adopted according to [19]. This model requires axial compressive behavior to account for the changes in nonlinear horizontal properties and frictional behavior for varying compressive load at each time step and have no tensile force carrying capability, and therefore, no horizontal force is generated when the isolators are in tension. Axial behavior is defined as nonlinear with effective stiffnesses calculated from the axial stiffness of the sliding puck for each type of isolator. Nonlinear horizontal behavior is coupled for two orthogonal directions and defined by five parameters: initial elastic stiffness $K_1$, friction coefficient at zero (slow) velocity $f_{min}$, friction coefficient at high velocity $f_{max}$, rate parameter $a$, which is a constant for given bearing pressure and condition of sliding surface, and the net pendulum radius $R$. The velocity dependence of friction coefficient is determined by equation (1), where $\dot{u}$ is the sliding velocity at that instant.

$$\mu = f_{max} - (f_{max} - f_{min})e^{-a|\dot{u}|} \tag{1}$$

The FPI model can estimate the behavior of friction isolators the most accurate in biaxial earthquake excitation conditions. Also, the model can represent the axial load dependency of the nonlinear stiffness and velocity dependency of friction coefficient. Therefore, the FPI model is selected as the primary tool for the design and analysis of FPS.

In addition, friction pendulum system isolators were also modeled as Multilinear Plastic (MLP) links with kinematic hysteretic model [15]. In this model, two orthogonal directions are uncoupled.

Therefore, the movement in the direction of one of the two main orthogonal axes is not affected by the earthquake excitation given in the transverse direction. In MLP link description, horizontal bilinear force deformation relationship, as shown in Figure 4, is the input parameter for nonlinear time-history analysis. When the isolator exceeds the yield displacement $D_y$, and yield force $F_y$, the horizontal stiffness of the isolators, $K_2$, is assigned as post-yield stiffness. Effective stiffness $K_{\text{eff}}$ and effective damping ratio $\xi$ were also introduced for modal superposition analysis. Axial behavior of the isolators was taken as linear elastic with corresponding axial compressive stiffness. Furthermore, this behavior cannot account for the gap behavior for the friction pendulum isolator devices, however, is widely used in structural engineering practices. Therefore, isolators are assumed to take tensile forces and horizontal stiffnesses do not depend on the variations in axial tension-compression behavior.

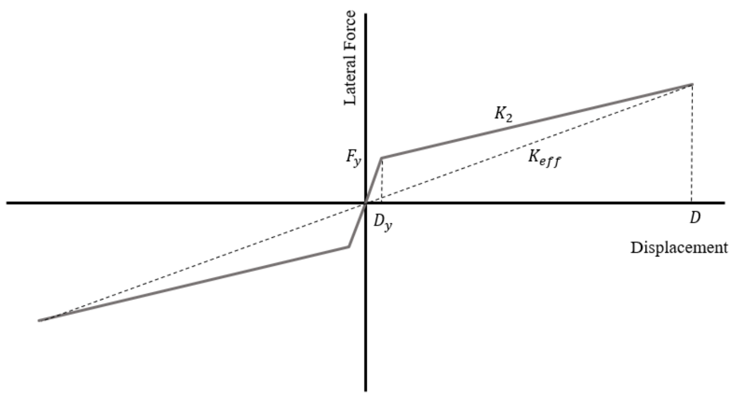


Figure 3. Bilinear force deformation relationship input for friction pendulum system

Modal analysis with nominal properties for DBE and MCE earthquake levels were conducted. Periods and modal participation ratios are given in Table 4. Total of 97% mass participation was obtained for both x and y directions in the first three modes.

Table 4. Modal properties of the building with FPS isolators

| | FPS-DBE | | | FPS-MCE | | |
|---|---|---|---|---|---|---|
| Mode | Period (s) | Mx | My | Period (s) | Mx | My |
| 1 | 3.041 | 0.694 | 0.064 | 3.949 | 0.715 | 0.064 |
| 2 | 2.979 | 0.071 | 0.896 | 3.883 | 0.074 | 0.910 |
| 3 | 2.82 | 0.202 | 0.008 | 3.689 | 0.195 | 0.011 |

## 2.3 Modeling of HDRB

In the analysis, deformation history integral type (DHI) model [6, 7, 8] which is the newly developed numerical model for high-damping rubber bearing, is used. As mentioned in **1.2**, HDRB has non-linearity in its shear stress-strain relationship. One of the typical characteristics is the hardening when shear strain generally exceeds 200%. Additionally, HDRB has cyclic stiffness degradation. In the cyclic loading, the shear stress of HDRB gradually decrease as number of cycle increase. Furthermore, the shear stress is relaxed and decreased when maximum experienced displacement is advanced during the deformation. These characteristics have not been sufficiently represented in the conventional HDRB modelling methods, such as bilinear model, which is widely used for modeling of elasto-plastic behavior of a structural element. Generally, the characteristics of the rubber is categorized as visco-elasticity. The representative studies in nonlinear viscoelastic models had been conducted by J.C.Simo [14]. One of the Simo's model represents the cyclic stress-strain behavior with generalized models of dashpot and spring. The model is time dependent and the stress is affected by strain rate. However, when the model is used to model HDRB characteristics, it was found that the rate dependent characteristics does not show agreement with experimental results. As many previous test results indicate, the HDRB has rate dependent characteristics. However, when we identify the Simo's model by experiments, the velocity dependency on the restoring force characteristics is overestimated.

In the DHI model, the velocity dependent part of Simo's equation is modified as strain (displacement) history dependent. The restoring force characteristics of HDRB consist of a elastic spring element and multiple elements of hysteretic spring element. The physical concept and mathematical expression of the model of a pair of elastic and hysteretic spring is shown in Figure 5, and mathematic expression of unit element the basic form of constitutive law is expressed in equation (2). The model has been implemented in the nonlinear link element of ETABS since version 17. In the ETABS, model consists of one elastic spring and two hysteretic springs.

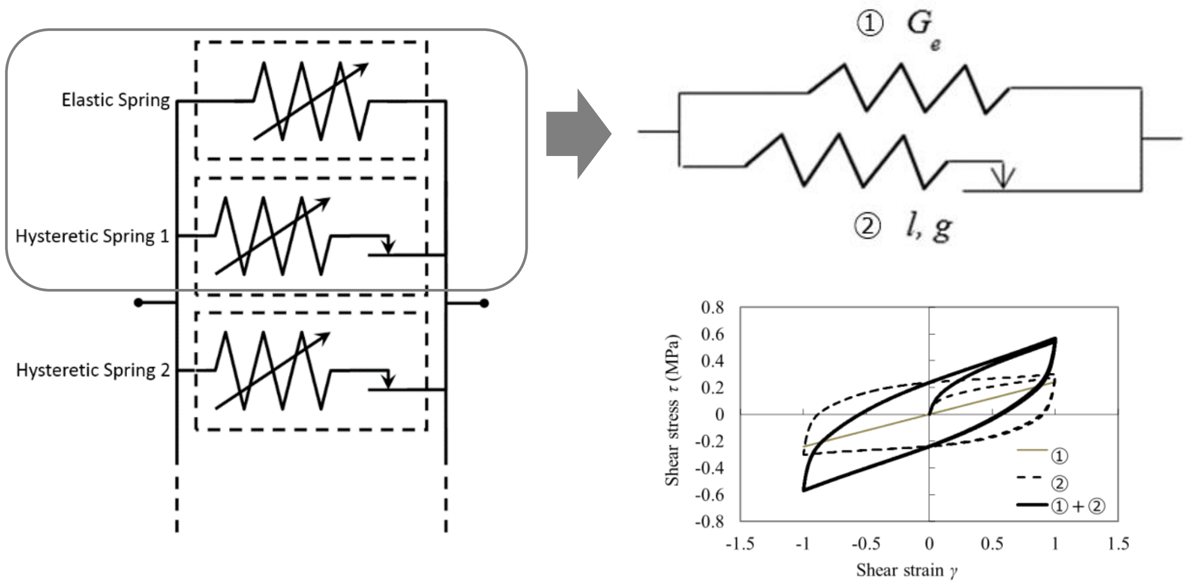


Figure 4. Concept of DHI model: Bi-directional numerical model for HDRB

$$
\begin{aligned}
\tau_x(\gamma_x, \gamma_y) &= \Xi(t) G_e \gamma_x \\
&\quad + \sum_i^n g_i \int_0^{\Gamma} e^{-(\Gamma-\Gamma')/l_i} \frac{d}{d\Gamma'} \left[ \frac{1}{3} \left( \gamma_x' - \gamma_x \right) \left( {\gamma_x'}^2 + {\gamma_y'}^2 \right) + \gamma_x' \right] d\Gamma' \\
\tau_y(\gamma_x, \gamma_y) &= \Xi(t) G_e \gamma_y \\
&\quad + \sum_i^n g_i \int_0^{\Gamma} e^{-(\Gamma-\Gamma')/l_i} \frac{d}{d\Gamma'} \left[ \frac{1}{3} \left( \gamma_y' - \gamma_y \right) \left( {\gamma_x'}^2 + {\gamma_y'}^2 \right) + \gamma_y' \right] d\Gamma'
\end{aligned} \tag{2}
$$

$$
\Xi(t) = \theta + (1 - \theta) \exp\left( - \frac{\gamma_m(t)}{\gamma_d} \right)
$$

where,

$$
\Gamma = \int_C \sqrt{d\gamma_x^2 + d\gamma_y^2}
$$

$$
\gamma_m(t) = \max_t \left[ \sqrt{{\gamma_x}^2 + {\gamma_y}^2} \right]
$$

$\gamma_x, \gamma_y$ : shear strain in x, y direction

$\tau_x, \tau_y$ : shear stress in x, y direction

$\Gamma$ : curvilinear integral along the deformation orbit C on $\gamma_x$-$\gamma_y$ plane

$l_i, g_i, G_e, \theta, \gamma_d$ : material parameters

$\Xi(t)$ : damage function ( degradation of stiffness by loading history)

In the isolation of the hospital building model, three types of HDRB isolators were selected based on the column axial compressive loads. Design displacements for MCE and DBE levels were determined as 54 cm and 25 cm which corresponds to shear strains of 270% and 125%, respectively. Axial compressive behavior of HDRB isolators were modeled elastically and independent of shear behavior. The nominal shear properties of isolators at maximum shear strain of 270% are summarized in Table 5. Stiffness property modification factors for upper and lower bound (UB and LB) were specified by Bridgestone as 1.45 and 0.9. Corresponding modification factors for effective damping are also provided as 0.94 and 0.9, respectively.

The DHI model can estimate the behavior of HDRBs under biaxial earthquake excitation conditions. Also, it can model the nonlinear stiffness increase when the shear strain exceeds 250%. Therefore, in this study, the DHI model is selected as the primary mathematical model for the design and analysis of high damping rubber bearings.

Table 5. Mechanical properties of selected HDRB isolators [20]

| **Property** | **Type1** | **Type2** | **Type3** |
|---|---|---|---|
| # of iso. | 83 | 15 | 20 |
| $D$ (mm) | 1000 | 1100 | 1200 |
| $A$ (mm2) | 784900 | 948000 | 1128600 |
| $H$ (mm) | 201 | 200 | 200 |
| $K_v$ (kN/m) | 5450000 | 6590000 | 7860000 |
| $G_{eq}$ (MPa) | 0.495 | 0. 495 | 0. 495 |
| $K_{eq}$ (kN/m) | 1932.5 | 2345.7 | 2792.6 |

| | | | |
|---|---|---|---|
| $H_{eq}$ | 0.194 | 0.194 | 0.194 |
| $D_{tm}$ (mm) | 542.7 | 540 | 540 |
| $K_2$=$K_1$/10 (kN/m) | 1309.9 | 1590.0 | 1892.9 |

Material shear stress-strain properties are input parameters to ETABS analysis software in order to construct nonlinear force deformation behavior of high damping rubber isolator link modeling approach (i.e. DHI model) as can be seen in Figure 5. These parameters were specified by Bridgestone and shown in Table 6.

Table 6. Material input parameters for DHI model

| Property | Nominal | UB | LB |
|---|---|---|---|
| Added Elastic Stiffness – $G_e$ (MPa) | 0.5257 | 0.8136 | 0.5262 |
| Control Strength 1 - $g_1$ (MPa) | 2.468 | 3.364 | 1.999 |
| Control Strength 2 - $g_2$ (MPa) | 0.3564 | 0.4858 | 0.2887 |
| Control Strain 1 - $l_1$ | 0.03591 | 0.03591 | 0.03591 |
| Control Strain 2 - $l_2$ | 0.5 | 0.5 | 0.5 |
| Resistance Ratio - $\theta$ | 0.4598 | 0.4598 | 0.4598 |
| Damage Parameter – $\gamma_d$ | 0.4181 | 0.4181 | 0.4181 |

As a second approach for modeling the high damping rubber bearings, Hysteretic Rubber Isolator (RI) links implemented in ETABS [15] were used. This plasticity model is based on the theories in [17] and [18] and recommended in [16] for base isolation applications. The nonlinear behavior in two degrees of freedom for shear is coupled and are independent from the axial force. Therefore, this model can also estimate the behavior under bi-directional earthquake excitation. Nonlinear horizontal behavior is defined by three parameters: initial elastic stiffness $K_1$, yield strength $Q_d$ and the ratio of post-yield stiffness to initial stiffness $K_2/K_1$ as in the Figure 6.

In the third modeling approach, bilinear force deformation relationship of HDRB isolators were estimated from mechanical properties, shown in Table 6, and idealized as bilinear Multi Linear Plastic links (MLP) in the building model as shown with the dashed lines in Figure 5.

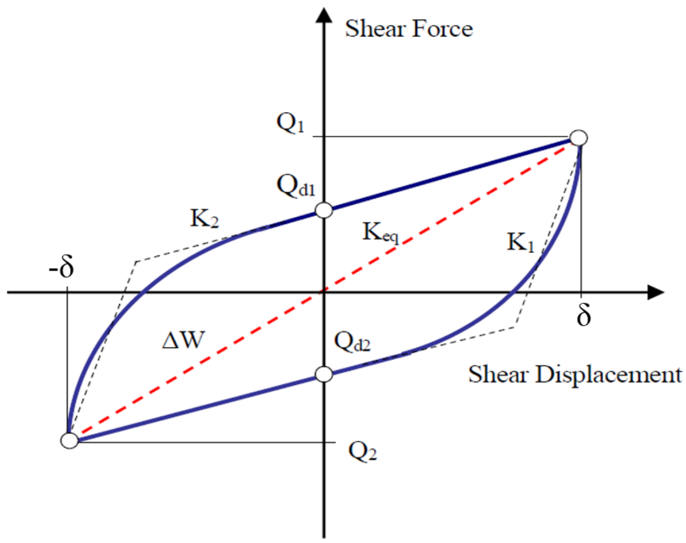


Figure 5. Nonlinear force deformation behavior of HDRB

Modal analysis of DBE with UB and MCE with LB parameters were conducted. Periods and modal mass participation ratios ($M_y$ and $M_y$) are given in Table 7. Total of 99% mass participation was obtained for both x and y directions in the first three modes.

Table 7. Modal properties of the building with HDRB isolators

| | HDRB-DBE-UB | | | HDRB-MCE-LB | | |
|---|---|---|---|---|---|---|
| Mode | Period (s) | Mx | My | Period (s) | Mx | My |
| 1 | 2.734 | 0.696 | 0.077 | 3.364 | 0.738 | 0.076 |
| 2 | 2.682 | 0.079 | 0.881 | 3.312 | 0.080 | 0.903 |
| 3 | 2.499 | 0.189 | 0.005 | 3.094 | 0.167 | 0.006 |

## 3 ANALYSIS

As specified in Turkish Building Seismic Code, for each isolator type, maximum considered earthquake (MCE) and design basis earthquake (DBE) level analyses were conducted. Maximum isolator displacements were determined under the MCE level analysis with lower bound isolator properties. DBE level analyses with upper bound isolator properties were conducted to obtain maximum forces acting on superstructure. Story accelerations and interstory drifts were obtained and compared under DBE earthquake level with nominal isolator properties.

For each DBE and MCE level analysis, target response spectrum is introduced to the analysis software as 100% in main direction and 30% in the orthogonal direction (i.e. $E_{X,Y} = E_{x,y}+0.3E_{y,x}$) according to the code. Response spectrum analysis results are obtained by modal combination of both x and y direction. To account for damping effects in response spectrum analysis, linear effective damping values were estimated by using the mechanical properties of isolators and assigned as the isolator effective damping along with the effective stiffness.

Acceleration record of two main orthogonal components of each ground motion are assigned as time-history functions and combined by scaling with the factors given in Table 2. Two pairs of time history analysis were created by interchanging the directions of each ground motion components in order to conduct the analysis under the most unfavorable case possible. Nonlinear modal time history analysis [15] method was used instead of the direct integration method due to the limitations on computational power.

Maximum isolator displacements are checked, and nonlinear isolator properties were modified with an iterative manner until displacement convergence with the design displacement is achieved for both isolator types.

## 4 RESULTS

Equivalent lateral force procedure, modal superposition and nonlinear time-history analysis results are discussed in this section. First, displacements and reactions obtained using ELFP and modal superposition analysis results are summarized. Later in this section, floor accelerations, story drifts and isolator hysteretic responses were also examined in detail, under nonlinear time-history analyses. A comparison of analysis results is made with respect to the ELFP according to Turkish Building Seismic Code.

In the tables given in Appendix B, for each link model, maximum isolator displacement and base shear coefficient results of both time-history (at the top) and response spectrum (at the bottom) analyses are presented. Displacements were obtained from the maximum and minimum isolator deformation for the isolation floor interface. For time history analysis, isolator displacements were obtained as 55.4 cm for HDRB and 64.3 cm for FPS isolators. Displacements are not multiplied by the coefficients due to torsional effects. Moreover, base shear coefficients obtained from both HDRB and FPS types were close and slightly lower than 0.2. HDRB isolators yielded lower displacements but higher base shear forces than FPS isolators due to higher total stiffness. Displacements and reactions reduced slightly when the isolator model type is changed to RI and MLP links and the reason will be discussed in later sections over the relevant hysteresis curves. Significantly lower displacements and base shear coefficients were obtained when response spectrum analysis is used including the effective damping.

Equivalent lateral force procedure proposed in Turkish seismic code was conducted for both HDRB and FPS isolators in order to compare displacement and base shear demands. The structure was assumed as a single degree of freedom system and the total stiffness of the isolation level was used in the calculations which are given in Table 8 and Table 9 for MCE with lower bound and DBE with upper bound properties, respectively. In general, FPS isolators show significantly higher maximum isolator displacements. On the other hand, base shear demands are %20 higher for HDRB case due to the total stiffness difference between FPS and HDRB.

Table 8. ELF procedure with MCE-lower bound properties

| | **HDRB** | **FPS** |
|---|---|---|
| **Total Effective Weight (kN), $\boldsymbol{W}$** | 492384 | |
| **Total Stiffness (kN/m), $\boldsymbol{K_M}$** | 226292.7 | 159076.7 |
| **Period (s), $\boldsymbol{T_M = 2\pi\sqrt{\frac{W}{gK_M}}}$** | 2.959 | 3.529 |

| | | |
|---|---|---|
| **Damping Ratio (%), $\xi$** | 19.4 | 18.6 |
| **Damping Scale, $\eta = \sqrt{\frac{10}{5+\xi}}$** | 0.640 | 0.651 |
| **Spectral Acc. (g), $S_{ae}^{DD-1}(T_M)$** | 0.310 | 0.261 |
| **Displacement (m),** $D_M = 1.3\left(\frac{g}{4\pi^2}\right)T_M^2\eta_M S_{ae}^{DD-1}(T_M)$ | 0.561 | 0.685 |

Table 9. ELF procedure with DBE-upper bound properties

| | **HDRB** | **FPS** |
|---|---|---|
| **Total Weight (kN), $W$** | 492384 | |
| **Total Stiffness (kN/m), $K_D$** | 407459.9 | 330034.9 |
| **Period (s), $T_D = 2\pi\sqrt{\frac{W}{gK_D}}$** | 2.205 | 2.450 |
| **Damping Ratio (%), $\xi$** | 23.6 | 30 (Max) |
| **Damping Scale, $\eta = \sqrt{\frac{10}{5+\xi}}$** | 0.590 | 0.534 |
| **Spectral Acc. (g), $S_{ae}^{DD-2}(T_D)$** | 0.241 | 0.217 |
| **Displacement (m),** $D_D = 1.3\left(\frac{g}{4\pi^2}\right)T_D^2\eta_D S_{ae}^{DD-2}(T_D)$ | 0.223 | 0.225 |
| **Base Shear Coefficient,** $C_D = \frac{V_D}{W} = \frac{K_D D_D}{W}$ | 0.185 | 0.151 |

Both HDRB and FPS designs were also analyzed by modal superposition procedure under the target response spectra. Response spectrum analysis results yielded lower displacements and higher base shear values for the HDRB, similar to the ELFP approach. The results are summarized in Table 10.

Table 10. Response spectrum (modal superposition) analysis results

| | **MCE** | | **DBE** | |
|---|---|---|---|---|
| | **HDRB** | **FPS** | **HDRB** | **FPS** |
| **Isolator Displacement (m)** | 0.410 | 0.528 | 0.162 | 0.179 |
| **Base Shear Coefficient (V/W)** | - | - | 0.127 | 0.105 |

In Turkish seismic code, the acceptability criteria of isolator displacements and base reactions for both response spectrum and nonlinear time history analyses are specified. In the code it is stated that the isolator displacements obtained from the response spectrum and nonlinear time history analyses cannot be taken lower than 0.9 times the displacements obtained from the equivalent lateral force procedure for structures with plan irregularities. Similar conditions apply for substructural and superstructural forces. Summary of isolator displacements and base shear coefficients obtained from four analysis approaches and corresponding criteria are given in Table 11 and Table 12, respectively. NLTH analysis results satisfy the code criteria and were used as the design values. For HDRB and FPS designs, MCE level earthquake with lower bound factors yielded 55.4 cm and 64.3 cm displacements, respectively. Base shear coefficients were obtained as 0.195 and 0.194 for DBE level earthquake with upper bound properties.

Table 11. Summary of isolator displacements for all analysis types

| | HDRB | FPS | Check |
|---|---|---|---|
| $D_{M,ELF}$ (m) | 0.561 | 0.685 | |
| $D_{M,RS}$ (m) | 0.411 | 0.528 | $< 0.9D_{M,ELF}$ NOT OK! |
| $D_{M,NLTH}$ (m) | 0.554 | 0.643 | $\geq 0.9D_{M,ELF}$ OK! |

Table 12. Summary of base shear coefficients for all analysis types

| | HDRB | FPS | Check |
|---|---|---|---|
| $C_{D,ELF}$ | 0.185 | 0.151 | |
| $C_{D,RS}$ | 0.127 | 0.105 | $< 0.9C_{D,ELF}$ NOT OK! |
| $C_{D,NLTH}$ | 0.195 | 0.194 | $\geq 0.9C_{D,ELF}$ OK! |

## 4.1 Nonlinear Time-History Analysis

Maximum isolator displacements under seven ground motions at MCE lower bound and DBE upper bound properties are shown in Figures 7a and 7b for DHI and FPI isolator link models. For MCE earthquake level, average isolator displacement of each ground motion is 55.4 cm and 64.3 cm for HDRB and FPS isolators, respectively. Lower displacements were obtained when RI and MLP link models were used. Furthermore, in DBE analyses, as 24.4 cm and 22.4 cm results were obtained for HDRB and FPS, respectively.

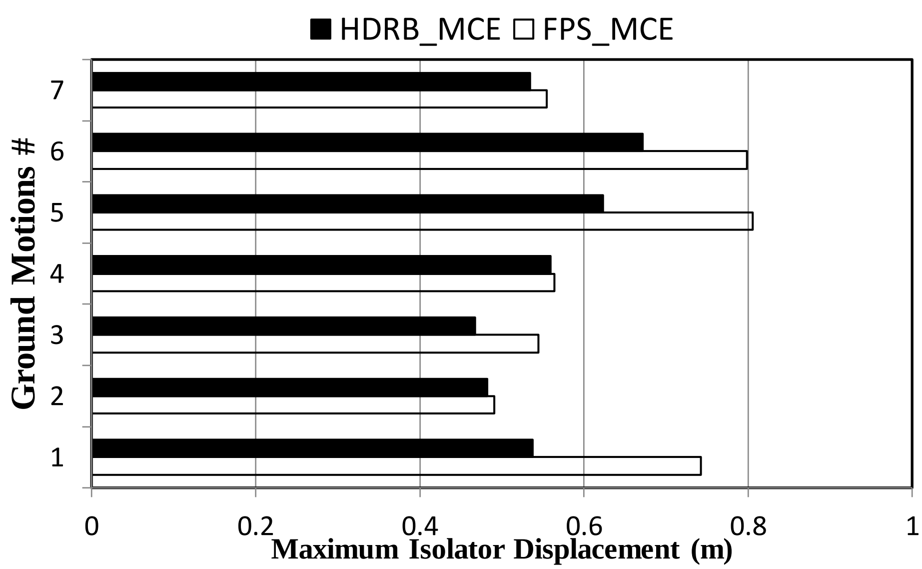


Figure 6a. Maximum isolator displacements at DBE level using upper bound properties obtained by nonlinear time-history analysis

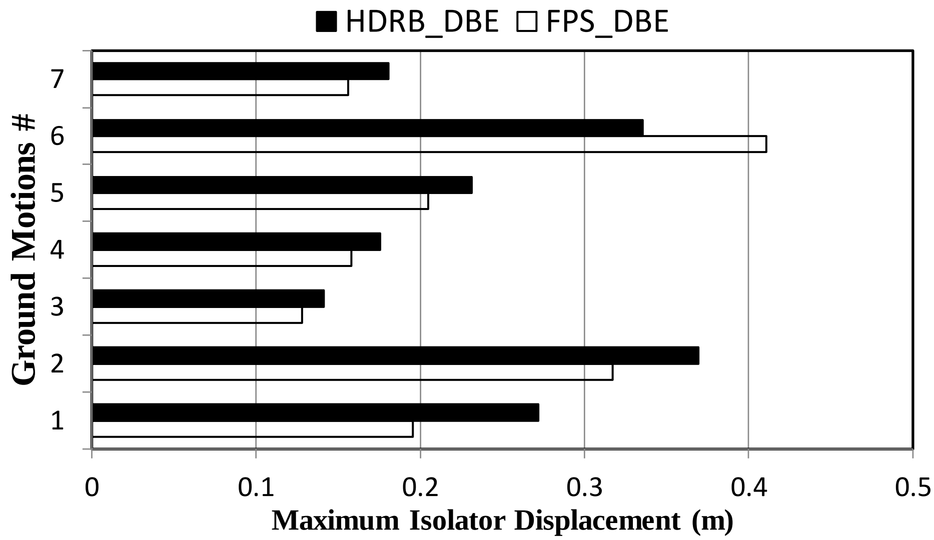


Figure 6b. Maximum isolator displacements at MCE level using lower bound obtained by nonlinear time-history analysis

Base shear coefficients for DBE earthquake level for each ground motion is also compared and presented in Figure 8 for DHI and FPI link models. The average base shear coefficients of seven ground motions are 0.195 and 0.194 for HDRB and FPS, respectively. There is big difference in base shear coefficients in the ground motion #2, as HDRB isolators show higher displacements, in Figure 7a, and have higher total stiffness, that results in amplified base shear forces, which are higher than that of FPS.

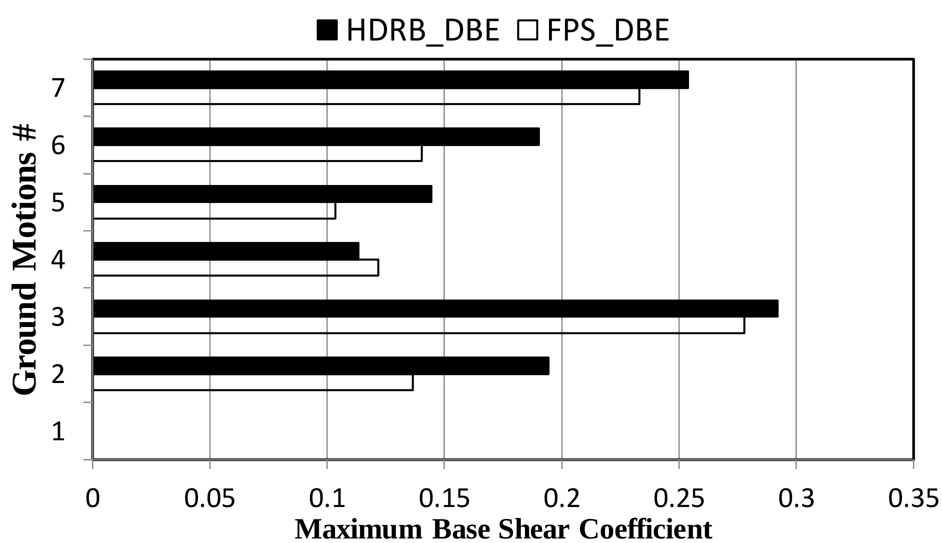


Figure 7. Maximum base shear coefficients at DBE obtained from nonlinear time-history analysis

## 4.2 Floor Accelerations

The maximum floor accelerations were obtained from the points which are located at the very edge of the T plan sections. The average of maximum floor accelerations of seven ground motions are compared in Figure 9a and 9b for DBE analyses with nominal factors. Floor 1 was taken as the story just above the isolation interface.

There are two components of the floor accelerations obtained in the figures. The first one is the translational acceleration of the building in the considered direction. Second one is the significant rotational accelerations in both main directions induced by high rotational participation in the dominant modes due to the T-shape plan eccentricity of the building.

HDRB isolators yielded relatively lower floor accelerations when compared to FPS. The DHI model gives the lowest results, nearly 0.2 g, except for the top floor. When RI model is used, the accelerations increase up to 0.3 g except for the top floor. Moreover, the FPI model of friction isolators also shows accelerations close to 0.25-0.35 g. These results could be acceptable for the design criteria 0.3 g limit, in hospital specifications, is considered.

Bilinear MLP modeling approach yielded accelerations as high as 0.4-0.7 g on this specific structure for both HDRB and FPS type isolators and should be questioned when used in the design. It is thought that two reasons can be associated with this phenomenon. First, the bilinear MLP model has relatively higher initial stiffness when compared to nonlinear initial stiffness of other modeling approaches. Therefore, the structure has smaller period, thus higher accelerations, when the isolators are in the elastic region in the MLP model. The second reason might be the sudden changes between elastic and post-yield stiffnesses resulting in amplified accelerations on the structure.

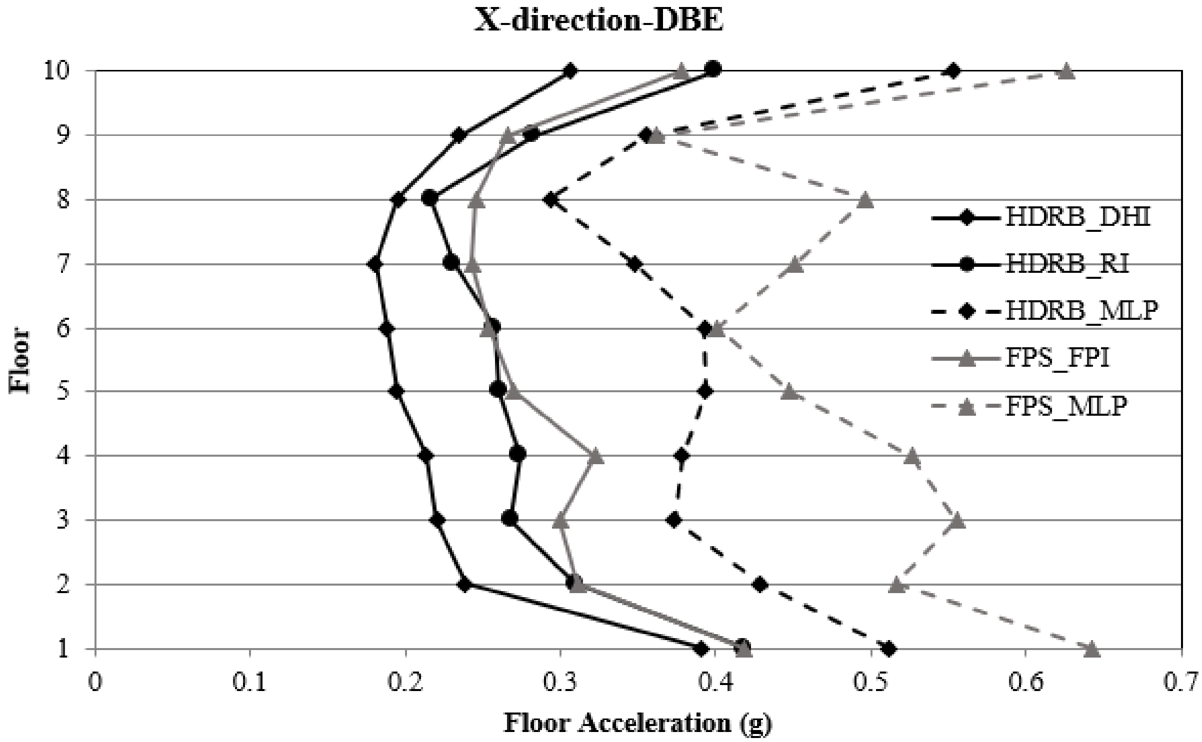


Figure 8a. Average floor accelerations for seven ground motions in X-direction

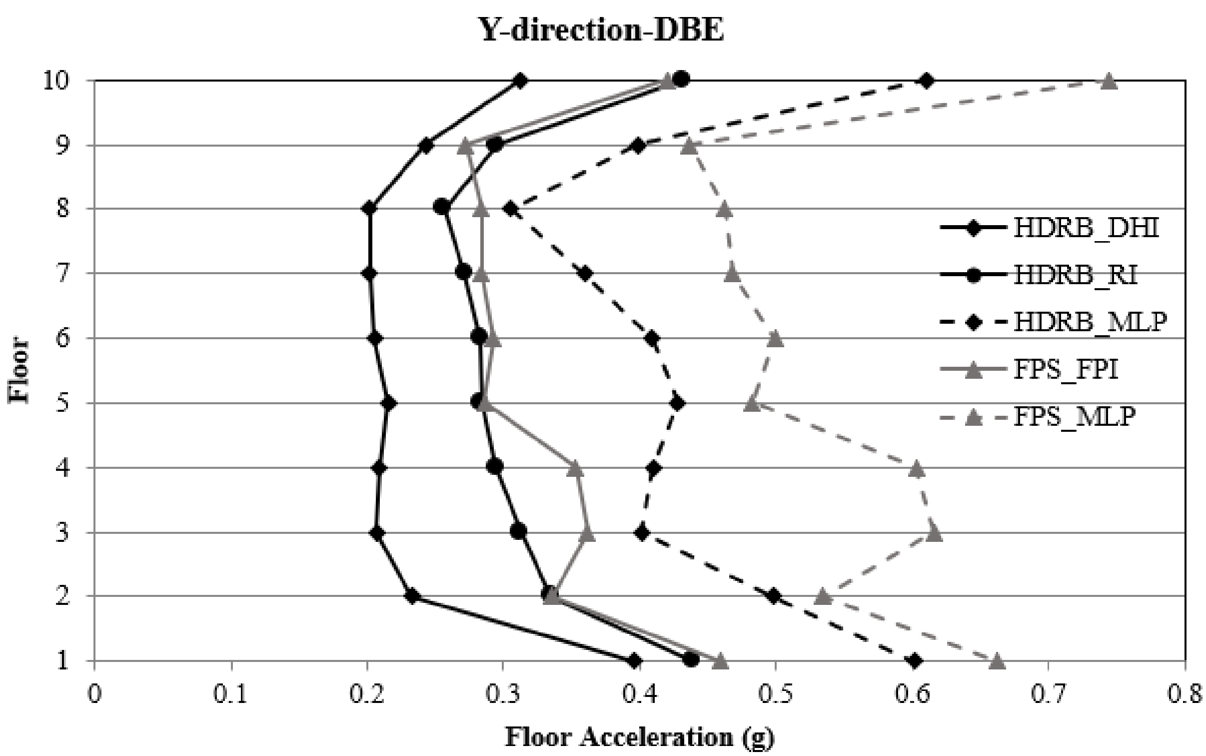


Figure 8b. Average floor accelerations for seven ground motions in Y-direction

## 4.3 Story Drifts

Maximum interstory drift ratios were obtained for each floor under DBE seismic level with nominal isolator parameters and presented in Figure 10. As the first floor was taken to be the top of the isolation interface, substantial drift ratio levels were obtained due to significant movement of the isolators relative to the floor below. Above this level, story drifts show an increasing trend up to the fourth floor and decrease from fourth to the top story. The story drift limit (0.5%) for the Turkish Building Seismic Code designated for the uninterrupted operation seismic performance level is also shown in the figures for comparison.

Very similar drifts ratios were obtained for DHI and FPI models, ranging between 0.2% and 0.4%, and satisfy the code limitations. Increased story drifts were attained when HDRB isolators modeled with RI links. Results of MLP link model show significantly higher story drifts and do not satisfy the code requirements between the 3rd and the 5th floor.

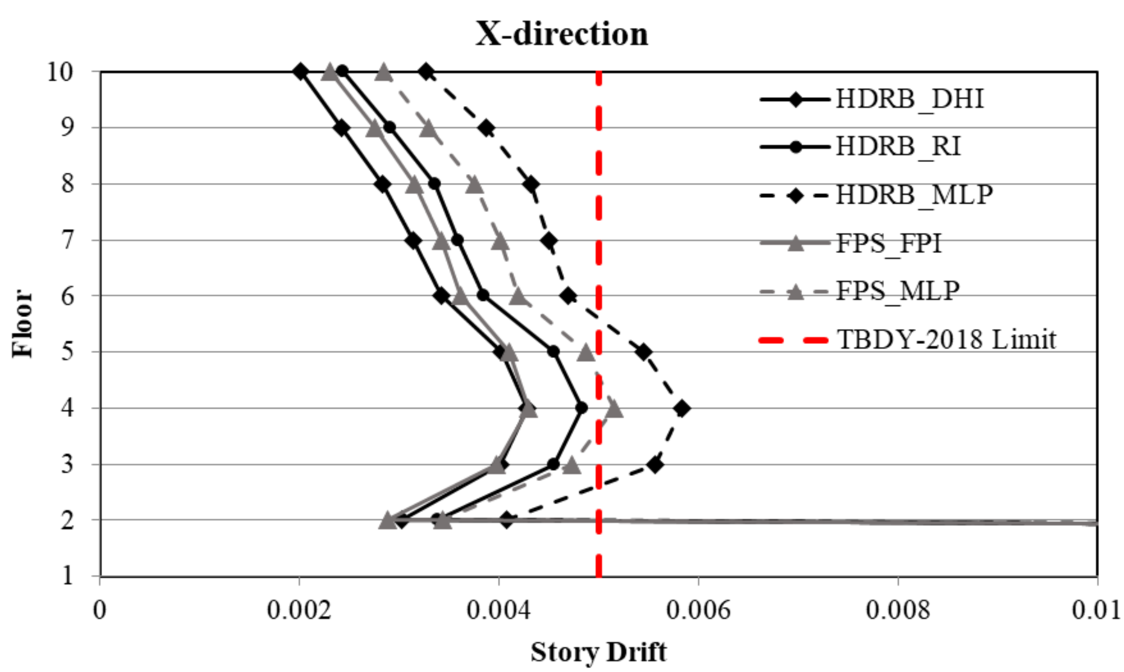


Figure 9a. Average story drifts for seven ground motions for X-direction

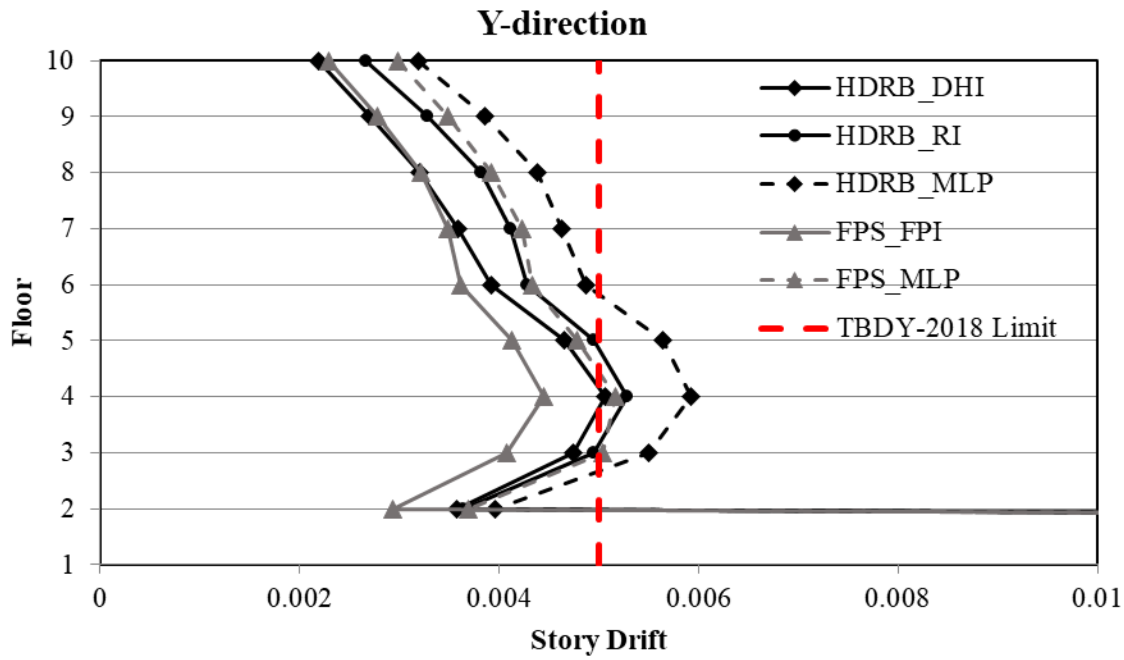


Figure 9b. Average story drifts for seven ground motions for Y-direction

### 4.4 Hysteretic Curves

For DHI, RI, FPI, and MLP link approaches, axial force history and horizontal force-deformation hysteretic behaviors of three isolators, at different locations of the building, are provided in Appendix C for the ground motion #4 (Kobe1116). Isolators were selected according to their axial load variations and their locations so that rotational effects at the isolators far from the stiffness center are more significant, and coupled directional behavior of isolators are clearly visible.

For all modeling approaches, isolators which are under or near the shear walls exhibit tensile or very high compressive forces during the earthquake due to the rocking motion of the shear walls. Similarly, isolators located at the perimeter axes of the T shaped plan, show a certain level of uplift or highly varying compressive forces because of the overturning moments acting on each arm of the T shape during the seismic motion.

In FPS-FPI links, quite limited frictional resisting force and energy dissipation were observed when the isolators are under relatively lower compressive stresses. Besides, during the uplift, no friction is generated, and energy dissipation becomes zero due to the compression dependency of nonlinear stiffness. The cycles, in which the highest displacements were observed in FPS, are occurred just after the uplift in most cases. When compared with idealized bilinear model, hysteresis behavior shows good agreement for the isolators under stable compression behavior. On the other hand, there is almost no agreement when the isolators show high variation in axial forces or uplift. The bilinear model could only estimate the displacements close but lower than the friction model since there is no change in energy dissipation for varying axial forces.

In this study uplift forces are neglected, and the axial load behavior of isolators is not reflected to the hysteresis curves for the mathematical models used for HDRBs. Bridgestone elastomeric isolators can bear small tensile stresses up to 1 MPa [20]. Therefore, for a design project, it is important to check whether the tensile loads exceed the isolator capacity during the earthquake if one of these models is used.

The DHI and RI model show very similar results for energy dissipation, maximum force, and displacement behavior except for some small difference in the nonlinear stiffness since the DHI model updates the stiffness at each displacement step. Both models could capture the effect of biaxial loading condition of earthquake ground motions. On the other hand, MLP links are able to show the general behavior of HDRBs. Lower displacements were obtained since two orthogonal directions are not coupled, and their reciprocal effect is not defined in the bilinear mathematical model.

## 5 CONCLUSIONS

A numerical study on a seismically isolated reinforced concrete hospital, designed according to older version of Turkish seismic code (2007), originally isolated with friction pendulum isolators was conducted to investigate the applicability of high damping rubber bearings. Equivalent lateral force procedure, nonlinear time-history analysis, and modal superposition analysis were conducted for performance comparison of the isolators. Different isolator models provided in the analysis software were used to show the effect of modeling techniques on earthquake response of the seismically isolated structure. Maximum isolator displacements, base shear coefficients, floor accelerations and story drift results were presented using two different earthquake levels, design basis earthquake (DBE) and maximum considered earthquake (MCE), with upper and lower bound factors used in the design. Comments were made according to the new Turkish Building Seismic

Code (2018). Based on the results, the following conclusions can be made for the investigated hospital building:

- Due to the higher total stiffness property, HDRB design yields lower maximum isolator displacements and higher base shear reactions than the FPS design for the same design displacement at MCE level earthquake with lower bound isolator parameters. Both isolator type shows similar base shear values.
- HDRB design with DHI modeling yielded relatively lower floor accelerations than FPS design with FPI links. Both designs showed acceptable acceleration results, lower than the 0.3g limit, stated in the relevant hospital specification. For RI and MLP models, the increase in rate of change of stiffness from elastic to post-yield results in amplified accelerations. The bilinear model generated excessively high accelerations that are not acceptable for the design.
- There are significant rotational accelerations as well as the translational accelerations due to the asymmetric plan shape (T shape) of the building for both isolator design. Therefore, when accelerations are concerned, the effect of rotational movement should not be ignored.
- Very similar interstory drift ratios were obtained for both isolator design with corresponding DHI and FPI models. When the link models are changed to RI and MLP, increased drift ratios were observed which could lead to results exceeding the code limits.
- The highest results among all performance parameters were obtained from nonlinear modal time-history analysis and these results can be used in the design. Modal superposition analysis, with linear damping introduced in the program, yielded quite low displacements and reactions that cannot be considerable in the design according to the Turkish Earthquake Code-2018 limitations, when compared relative to the equivalent lateral force procedure.
- The DHI and FPI models can capture the nonlinear behavior the best for HDRB and FPS isolators, respectively. Also, RI links could be an alternative and practical approach for modeling of elastomeric isolators in practice as the nonlinear behavior is captured well enough. The bilinear (MLP link) model lacks the ability to reflect the high nonlinearity in the behavior and biaxial loading of ground motions and may lead to unrealistic results especially when there is high axial force variation. The vertical earthquake components are neglected in this study. However, the new Turkish Building Seismic Code also requires

inputting the vertical ground motions, and clearly this will lead to increase in axial load variations, and thus tensile force demands on the isolators.

There is no significant superiority in performance found between two isolator designs for the considered hospital building. Both types could yield performance results that can be acceptable in the design if proper modeling approach is used. HDRBs can be preferred especially when there is a need for high energy absorption capability.

## 6 REFERENCES


[1] U. Akyuz, A. Caner, A. Yakut, S. Ozdemir, and N. Topkara, "A Comparative Study on Seismic Isolation Applications in Turkey", *Proceedings*, 2017 NZSEE Conference, April, Wellington, New Zealand, 2017.

[2] Kelly, J. M. (1996), *Earthquake –Resistant Design with Rubber*, 2nd ed., Springer-Verlag, London

[3] W.H. Robinson and A. G. Tucker, "Test Results for Lead-Rubber Bearings for the William M. Clayton Building, Toe Toe Bridge, and Waiotukupuna Bridge" *Bull. New Zealand Natl.Sc. Eng*., Vol. 14, 21-23, 1983

[4] V. Zayas, S. Low, L. Bozzo, and S. Mahin, "Feasibility and Performance Studies on Improving the Earthquake Resistance of New and Existing Buildings Using the Friction Pendulum System", University of California at Berkeley, Earthquake Engineering Research Center, Report No. UCB/EERC-89/09, 1989.

[5] C.J. Derham, J. M. Kelly, and A. G. Thomas, "Nonlinear Natural Rubber Bearings for Seismic Isolation", *Nuclear Eng. Design*, Vol. 84, No. 3, pp.417-428, 1985

[6] T. Mori, H. Kato and N. Murota, "FEM Analysis of High Damping Laminated Rubber Bearings Using an Elastic-Plastic Constitutive Law of the Deformation History Integral Type", *Journal of Structural and Construction Engineering*, vol.75, no. 658, pp. 2171-2178, 2010, (in Japanese).

[7] H. Kato, T. Mori, N. Murota and M. Kikuchi, “Analytical Model for Elastoplastic and Creep-Like Behavior of High-Damping Rubber Bearings,” *Journal of Structural Engineering*, vol. 141, no. 9, Sep. 2015.

[8] M. Masaki, T. Mori, N. Murota, and K. Kasai, “Validation of Hysteresis Model of Deformation-History Integral Type for High Damping Rubber Bearings”, presented at the 16th World Conference on Earthquake Engineering, Proceedings, 2017, Santiago, Chile.

[9] *ETABS 18 (v18.0.2),* Computers & Structures Inc., Berkeley, California, USA. Accessed: Dec. 2019.

[10] *Turkish Building Earthquake Code,* Presidency of Disaster and Emergency Management, Ministry of Interior, Turkey, 2018.

[11] *GeoScience Map Viewer and Drawing Editor,* General Directorate of Mineral Research and Exploration of Turkey, (2016). Available: http://yerbilimleri.mta.gov.tr/anasayfa.aspx

[12] C. M. Galindo, T. Spuler, G. Moor, and T. Stirnimann, “F. Design, Full-scale Testing and CE Certification of Anti-seismic Devices According to the New European Norm EN 15129: Curved Surface Sliders”, presented at the 15th World Conference on Earthquake Engineering, Lisbon, Portugal, 2012.

[13] *Specification for Structures to be Built in Disaster Areas*, Ministry of Public Works and Settlement, Turkey, 2007.

[14] J. C. Simo and T. J. R. Hughes (1997), Computational Inelasticity, Springer.

[15] *CSI Analysis Reference Manual for SAP2000, ETABS, SAFE and CSiBridge,* Computers & Structures Inc., USA, 2017.

[16] S. Nagarajaiah, A. M. Reinhorn, and M. C. Constantinou, “Nonlinear Dynamic Analysis of 3-D Base-Isolated Structures”, *Journal of Structural Engineering*, vol. 117, no. 7, pp. 2035-2054, 1991.

[17] Y. K. Wen, “Method for Random Vibration of Hysteretic Systems,” *Journal of the Engineering Mechanics Division*, vol. 102, no. EM2, 1976.

[18] Y. J. Park, Y. K. Wen, A. H-S. Ang, "Random Vibration of Hysteretic Systems under Bi-Directional Ground Motions," *Earthquake Engineering and Stuctural Dynamics*, vol. 14, 1986.

[19] V. Zayas and S. Low "A Simple Pendulum Technique for Achieving Seismic Isolation," *Earthquake Spectra*, vol. 6, no. 2, 1990.

[20] *Seismic Isolation Product Line-up*, Bridgestone Corporation, Japan, n.d.

# 7 APPENDIX A

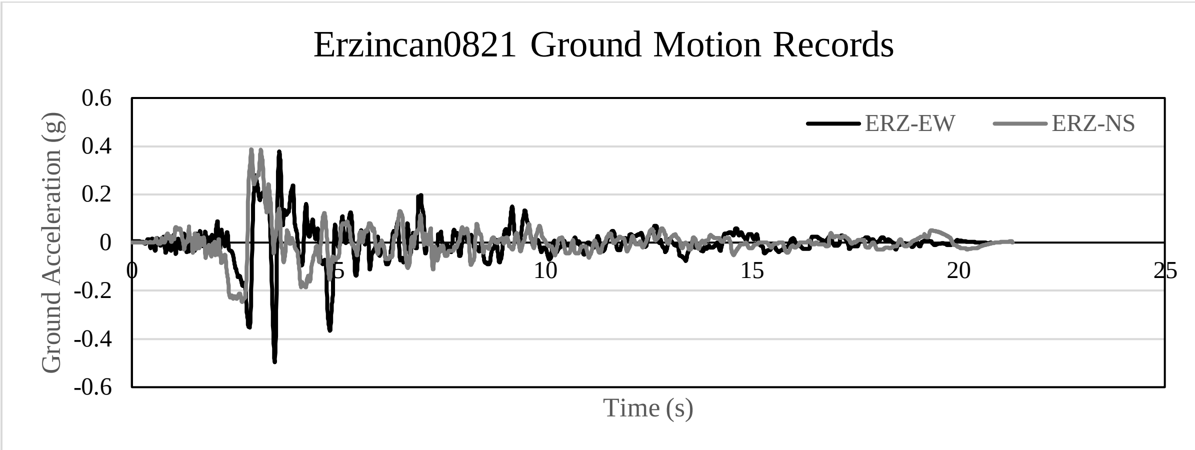


Figure 10. Acceleration records for both main directions for Erzincan0821 earthquake

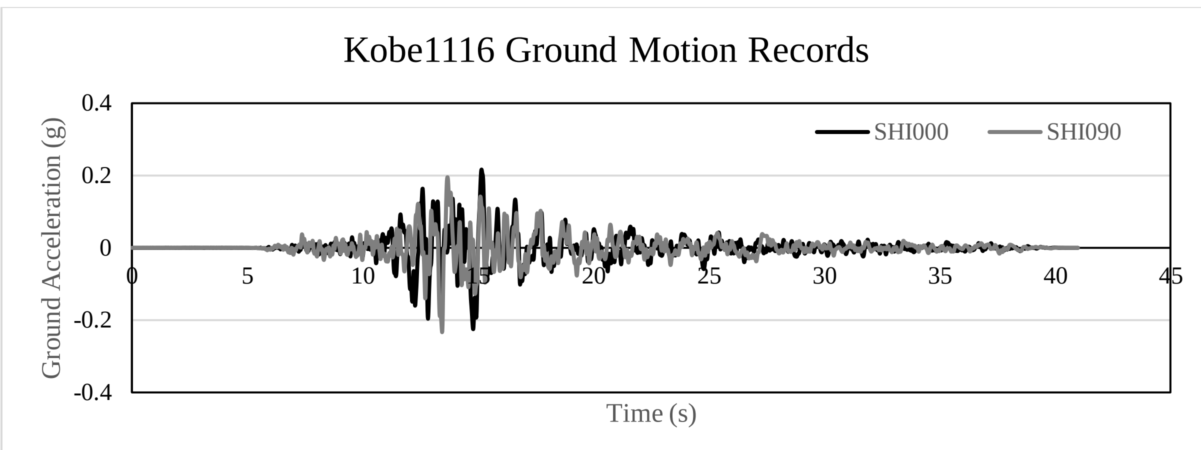


Figure 11. Acceleration records for both main directions for Kobe1116 earthquake

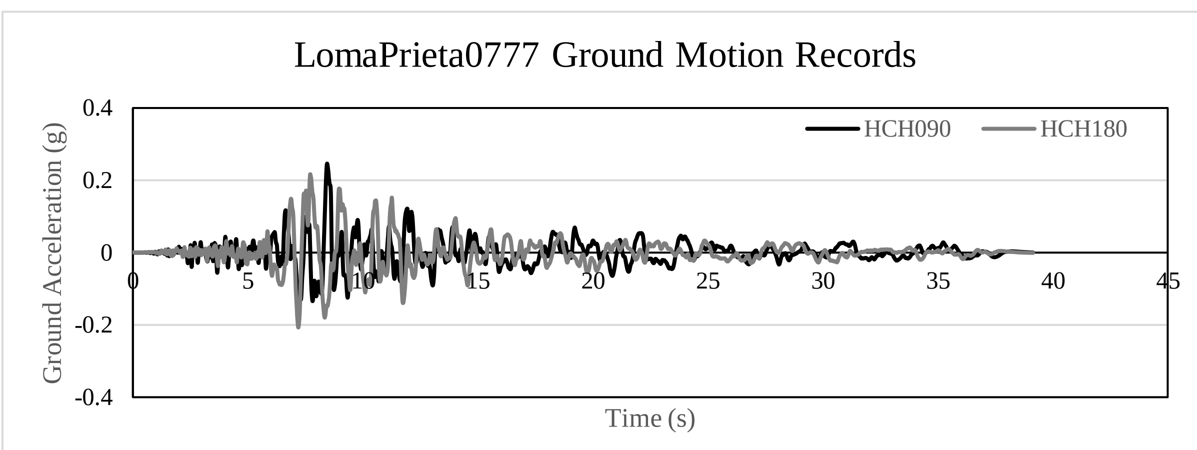


Figure 12. Acceleration records for both main directions for LomaPrieta0777 earthquake

# 8 APPENDIX B

Maximum isolator displacement and base shear coefficients obtained from each analysis are shown in Table 13, Table 14 and Table15.

Table 13. MCE-LB Isolator displacement results for response spectrum and time history analyses

| | Dm=0.54 m | | | | | | Dm=0.64 m | | | |
|---|---|---|---|---|---|---|---|---|---|---|
| **EQ No-** | **HDRB-DHI** | | **HDRB-RI** | | **HDRB_MLP** | | **FPS_FPI** | | **FPS_MLP** | |
| **Pair No** | **Ux (m)** | **Uy (m)** | **Ux (m)** | **Uy (m)** | **Ux (m)** | **Uy (m)** | **Ux (m)** | **Uy (m)** | **Ux (m)** | **Uy (m)** |
| **1-1 Max** | 0.305 | 0.537 | 0.171 | 0.468 | 0.156 | 0.443 | 0.326 | 0.743 | 0.216 | 0.639 |
| **1-1 Min** | -0.358 | -0.330 | -0.257 | -0.284 | -0.228 | -0.327 | -0.448 | -0.497 | -0.257 | -0.352 |
| **1-2 Max** | 0.516 | 0.304 | 0.458 | 0.188 | 0.414 | 0.159 | 0.707 | 0.350 | 0.631 | 0.233 |
| **1-2 Min** | -0.347 | -0.339 | -0.257 | -0.255 | -0.283 | -0.260 | -0.486 | -0.431 | -0.362 | -0.275 |
| **2-1 Max** | 0.350 | 0.474 | 0.229 | 0.402 | 0.278 | 0.388 | 0.290 | 0.491 | 0.257 | 0.437 |
| **2-1 Min** | -0.361 | -0.482 | -0.389 | -0.551 | -0.369 | -0.548 | -0.394 | -0.490 | -0.370 | -0.503 |
| **2-2 Max** | 0.477 | 0.369 | 0.421 | 0.274 | 0.405 | 0.253 | 0.490 | 0.313 | 0.459 | 0.296 |
| **2-2 Min** | -0.468 | -0.390 | -0.534 | -0.460 | -0.544 | -0.449 | -0.483 | -0.399 | -0.492 | -0.405 |
| **3-1 Max** | 0.464 | 0.322 | 0.343 | 0.303 | 0.241 | 0.296 | 0.521 | 0.377 | 0.470 | 0.296 |
| **3-1 Min** | -0.336 | -0.462 | -0.277 | -0.400 | -0.279 | -0.431 | -0.335 | -0.491 | -0.331 | -0.487 |
| **3-2 Max** | 0.339 | 0.467 | 0.307 | 0.334 | 0.275 | 0.252 | 0.393 | 0.544 | 0.294 | 0.460 |
| **3-2 Min** | -0.458 | -0.331 | -0.398 | -0.286 | -0.419 | -0.287 | -0.488 | -0.351 | -0.451 | -0.316 |
| **4-1 Max** | 0.496 | 0.423 | 0.491 | 0.469 | 0.456 | 0.380 | 0.487 | 0.461 | 0.479 | 0.437 |
| **4-1 Min** | -0.549 | -0.359 | -0.546 | -0.343 | -0.471 | -0.304 | -0.567 | -0.386 | -0.528 | -0.328 |
| **4-2 Max** | 0.359 | 0.509 | 0.387 | 0.486 | 0.346 | 0.483 | 0.450 | 0.512 | 0.416 | 0.484 |
| **4-2 Min** | -0.337 | -0.559 | -0.338 | -0.556 | -0.293 | -0.466 | -0.391 | -0.564 | -0.317 | -0.581 |
| **5-1 Max** | 0.629 | 0.284 | 0.512 | 0.339 | 0.503 | 0.351 | 0.776 | 0.323 | 0.669 | 0.365 |
| **5-1 Min** | -0.509 | -0.206 | -0.403 | -0.247 | -0.375 | -0.241 | -0.696 | -0.181 | -0.609 | -0.163 |
| **5-2 Max** | 0.276 | 0.623 | 0.317 | 0.508 | 0.325 | 0.504 | 0.312 | 0.806 | 0.342 | 0.676 |
| **5-2 Min** | -0.194 | -0.472 | -0.223 | -0.383 | -0.234 | -0.377 | -0.166 | -0.704 | -0.169 | -0.608 |
| **6-1 Max** | 0.376 | 0.223 | 0.390 | 0.229 | 0.401 | 0.382 | 0.535 | 0.181 | 0.490 | 0.240 |
| **6-1 Min** | -0.664 | -0.280 | -0.697 | -0.219 | -0.637 | -0.151 | -0.794 | -0.342 | -0.763 | -0.243 |
| **6-2 Max** | 0.194 | 0.362 | 0.146 | 0.406 | 0.316 | 0.421 | 0.143 | 0.545 | 0.183 | 0.490 |
| **6-2 Min** | -0.253 | -0.672 | -0.213 | -0.693 | -0.100 | -0.638 | -0.318 | -0.799 | -0.270 | -0.769 |
| **7-1 Max** | 0.371 | 0.312 | 0.316 | 0.210 | 0.244 | 0.214 | 0.350 | 0.301 | 0.281 | 0.263 |
| **7-1 Min** | -0.385 | -0.534 | -0.182 | -0.553 | -0.208 | -0.605 | -0.367 | -0.554 | -0.254 | -0.577 |
| **7-2 Max** | 0.304 | 0.385 | 0.200 | 0.295 | 0.211 | 0.214 | 0.306 | 0.359 | 0.232 | 0.291 |
| **7-2 Min** | -0.539 | -0.359 | -0.529 | -0.201 | -0.554 | -0.232 | -0.556 | -0.367 | -0.569 | -0.275 |
| **AVERAGE** | **0.548** | **0.554** | **0.525** | **0.533** | **0.506** | **0.522** | **0.630** | **0.643** | **0.589** | **0.605** |
| | | | | | | | | | | |
| **RS-X** | 0.410 | 0.118 | 0.410 | 0.118 | 0.410 | 0.118 | 0.528 | 0.153 | 0.528 | 0.153 |
| **RS-Y** | 0.114 | 0.394 | 0.114 | 0.394 | 0.114 | 0.394 | 0.149 | 0.513 | 0.149 | 0.513 |

Table 14. DBE-UB Isolator displacement results for response spectrum and time history analyses

| | Dd=0.25 m | | | | | | Dd=0.23 m | | | |
|---|---|---|---|---|---|---|---|---|---|---|
| EQ No-Pair No | HDRB-DHI | | HDRB-RI | | HDRB_MLP | | FPS_FPI | | FPS_MLP | |
| | Ux (m) | Uy (m) | Ux (m) | Uy (m) | Ux (m) | Uy (m) | Ux (m) | Uy (m) | Ux (m) | Uy (m) |
| **1-1 Max** | 0.144 | 0.272 | 0.099 | 0.200 | 0.125 | 0.180 | 0.066 | 0.195 | 0.025 | 0.179 |
| **1-1 Min** | -0.136 | -0.133 | -0.096 | -0.160 | -0.063 | -0.164 | -0.141 | -0.180 | -0.143 | -0.180 |
| **1-2 Max** | 0.270 | 0.144 | 0.210 | 0.088 | 0.179 | 0.121 | 0.183 | 0.074 | 0.179 | 0.026 |
| **1-2 Min** | -0.128 | -0.146 | -0.147 | -0.115 | -0.162 | -0.085 | -0.187 | -0.171 | -0.209 | -0.155 |
| **2-1 Max** | 0.175 | 0.229 | 0.145 | 0.240 | 0.171 | 0.220 | 0.161 | 0.234 | 0.125 | 0.188 |
| **2-1 Min** | -0.211 | -0.370 | -0.250 | -0.356 | -0.200 | -0.348 | -0.200 | -0.317 | -0.171 | -0.313 |
| **2-2 Max** | 0.236 | 0.189 | 0.212 | 0.199 | 0.238 | 0.224 | 0.233 | 0.181 | 0.195 | 0.114 |
| **2-2 Min** | -0.355 | -0.254 | -0.350 | -0.300 | -0.358 | -0.232 | -0.310 | -0.217 | -0.322 | -0.211 |
| **3-1 Max** | 0.079 | 0.134 | 0.073 | 0.120 | 0.072 | 0.139 | 0.098 | 0.111 | 0.069 | 0.105 |
| **3-1 Min** | -0.067 | -0.141 | -0.073 | -0.139 | -0.107 | -0.168 | -0.098 | -0.128 | -0.114 | -0.152 |
| **3-2 Max** | 0.141 | 0.092 | 0.124 | 0.080 | 0.132 | 0.089 | 0.125 | 0.124 | 0.116 | 0.095 |
| **3-2 Min** | -0.143 | -0.074 | -0.140 | -0.088 | -0.152 | -0.112 | -0.135 | -0.126 | -0.132 | -0.132 |
| **4-1 Max** | 0.180 | 0.136 | 0.160 | 0.107 | 0.139 | 0.125 | 0.142 | 0.136 | 0.114 | 0.123 |
| **4-1 Min** | -0.166 | -0.113 | -0.134 | -0.089 | -0.127 | -0.087 | -0.072 | -0.116 | -0.043 | -0.073 |
| **4-2 Max** | 0.118 | 0.175 | 0.106 | 0.150 | 0.122 | 0.136 | 0.128 | 0.158 | 0.127 | 0.129 |
| **4-2 Min** | -0.103 | -0.164 | -0.075 | -0.129 | -0.065 | -0.119 | -0.106 | -0.074 | -0.068 | -0.073 |
| **5-1 Max** | 0.236 | 0.186 | 0.208 | 0.163 | 0.156 | 0.182 | 0.187 | 0.205 | 0.111 | 0.171 |
| **5-1 Min** | -0.145 | -0.168 | -0.122 | -0.175 | -0.133 | -0.189 | -0.141 | -0.127 | -0.143 | -0.154 |
| **5-2 Max** | 0.173 | 0.231 | 0.163 | 0.211 | 0.170 | 0.174 | 0.181 | 0.171 | 0.169 | 0.110 |
| **5-2 Min** | -0.162 | -0.154 | -0.173 | -0.130 | -0.178 | -0.142 | -0.135 | -0.172 | -0.137 | -0.158 |
| **6-1 Max** | 0.156 | 0.117 | 0.147 | 0.144 | 0.128 | 0.187 | 0.005 | 0.060 | 0.004 | 0.182 |
| **6-1 Min** | -0.336 | -0.111 | -0.315 | -0.095 | -0.300 | -0.071 | -0.409 | -0.129 | -0.370 | -0.102 |
| **6-2 Max** | 0.103 | 0.157 | 0.111 | 0.158 | 0.158 | 0.142 | 0.054 | 0.004 | 0.154 | 0.003 |
| **6-2 Min** | -0.105 | -0.335 | -0.094 | -0.313 | -0.062 | -0.303 | -0.126 | -0.411 | -0.084 | -0.385 |
| **7-1 Max** | 0.100 | 0.096 | 0.065 | 0.105 | 0.044 | 0.112 | 0.071 | 0.073 | 0.051 | 0.083 |
| **7-1 Min** | -0.086 | -0.181 | -0.080 | -0.147 | -0.087 | -0.140 | -0.058 | -0.156 | -0.054 | -0.132 |
| **7-2 Max** | 0.091 | 0.095 | 0.105 | 0.074 | 0.132 | 0.060 | 0.052 | 0.077 | 0.068 | 0.064 |
| **7-2 Min** | -0.169 | -0.087 | -0.143 | -0.096 | -0.139 | -0.102 | -0.161 | -0.062 | -0.126 | -0.073 |
| **AVERAGE** | **0.241** | **0.244** | **0.218** | **0.217** | **0.206** | **0.209** | **0.219** | **0.224** | **0.208** | **0.209** |
| | | | | | | | | | | |
| **RS-X** | 0.162 | 0.047 | 0.162 | 0.047 | 0.162 | 0.047 | 0.179 | 0.052 | 0.179 | 0.052 |
| **RS-Y** | 0.045 | 0.156 | 0.045 | 0.156 | 0.045 | 0.156 | 0.051 | 0.174 | 0.051 | 0.174 |

Table 15. DBE-UB base shear coefficient results for response spectrum and time history analyses

| | Dd=0.25 m | | | | | | Dd=0.23 m | | | |
|---|---|---|---|---|---|---|---|---|---|---|
| EQ No-Pair No | HDRB-DHI | | HDRB-RI | | HDRB_MLP | | FPS_FPI | | FPS_MLP | |
| | Cx (kN) | Cy (kN) | Cx (m) | Cy (m) | Cx (kN) | Cy (kN) | Cx (kN) | Cy (kN) | Cx (kN) | Cy (kN) |
| **1-1 Max** | 0.109 | 0.103 | 0.075 | 0.118 | 0.048 | 0.124 | 0.071 | 0.090 | 0.076 | 0.104 |
| **1-1 Min** | -0.106 | -0.218 | -0.069 | -0.158 | -0.085 | -0.136 | -0.028 | -0.098 | -0.010 | -0.107 |
| **1-2 Max** | 0.105 | 0.110 | 0.117 | 0.081 | 0.117 | 0.059 | 0.093 | 0.075 | 0.103 | 0.075 |
| **1-2 Min** | -0.216 | -0.106 | -0.157 | -0.070 | -0.133 | -0.085 | -0.093 | -0.028 | -0.107 | -0.008 |
| **2-1 Max** | 0.164 | 0.291 | 0.184 | 0.279 | 0.148 | 0.278 | 0.101 | 0.156 | 0.090 | 0.179 |
| **2-1 Min** | -0.134 | -0.185 | -0.113 | -0.163 | -0.124 | -0.164 | -0.077 | -0.116 | -0.070 | -0.112 |
| **2-2 Max** | 0.290 | 0.168 | 0.278 | 0.187 | 0.275 | 0.149 | 0.157 | 0.103 | 0.179 | 0.091 |
| **2-2 Min** | -0.184 | -0.136 | -0.162 | -0.118 | -0.167 | -0.129 | -0.115 | -0.077 | -0.112 | -0.068 |
| **3-1 Max** | 0.052 | 0.113 | 0.057 | 0.109 | 0.074 | 0.122 | 0.048 | 0.054 | 0.060 | 0.076 |
| **3-1 Min** | -0.064 | -0.109 | -0.052 | -0.092 | -0.050 | -0.104 | -0.050 | -0.055 | -0.036 | -0.060 |
| **3-2 Max** | 0.113 | 0.053 | 0.109 | 0.057 | 0.121 | 0.078 | 0.057 | 0.047 | 0.072 | 0.055 |
| **3-2 Min** | -0.110 | -0.066 | -0.090 | -0.051 | -0.101 | -0.052 | -0.049 | -0.052 | -0.062 | -0.047 |
| **4-1 Max** | 0.128 | 0.076 | 0.097 | 0.059 | 0.081 | 0.044 | 0.035 | 0.051 | 0.022 | 0.034 |
| **4-1 Min** | -0.143 | -0.089 | -0.117 | -0.081 | -0.103 | -0.093 | -0.068 | -0.064 | -0.068 | -0.073 |
| **4-2 Max** | 0.076 | 0.131 | 0.060 | 0.099 | 0.047 | 0.084 | 0.053 | 0.034 | 0.033 | 0.026 |
| **4-2 Min** | -0.089 | -0.145 | -0.080 | -0.118 | -0.089 | -0.103 | -0.061 | -0.072 | -0.067 | -0.071 |
| **5-1 Max** | 0.116 | 0.127 | 0.095 | 0.141 | 0.094 | 0.140 | 0.071 | 0.057 | 0.071 | 0.070 |
| **5-1 Min** | -0.188 | -0.145 | -0.146 | -0.124 | -0.119 | -0.119 | -0.086 | -0.095 | -0.063 | -0.101 |
| **5-2 Max** | 0.126 | 0.118 | 0.139 | 0.097 | 0.139 | 0.097 | 0.062 | 0.071 | 0.070 | 0.074 |
| **5-2 Min** | -0.141 | -0.188 | -0.120 | -0.147 | -0.121 | -0.124 | -0.089 | -0.087 | -0.100 | -0.057 |
| **6-1 Max** | 0.271 | 0.084 | 0.248 | 0.074 | 0.231 | 0.053 | 0.207 | 0.061 | 0.219 | 0.046 |
| **6-1 Min** | -0.113 | -0.084 | -0.110 | -0.084 | -0.092 | -0.127 | -0.002 | -0.016 | -0.002 | -0.092 |
| **6-2 Max** | 0.083 | 0.272 | 0.074 | 0.249 | 0.050 | 0.233 | 0.061 | 0.211 | 0.043 | 0.223 |
| **6-2 Min** | -0.083 | -0.116 | -0.082 | -0.112 | -0.126 | -0.094 | -0.015 | -0.003 | -0.090 | -0.003 |
| **7-1 Max** | 0.066 | 0.139 | 0.062 | 0.112 | 0.060 | 0.105 | 0.026 | 0.077 | 0.028 | 0.073 |
| **7-1 Min** | -0.075 | -0.069 | -0.047 | -0.080 | -0.027 | -0.087 | -0.034 | -0.030 | -0.011 | -0.037 |
| **7-2 Max** | 0.137 | 0.068 | 0.108 | 0.064 | 0.101 | 0.058 | 0.078 | 0.027 | 0.071 | 0.025 |
| **7-2 Min** | -0.069 | -0.074 | -0.080 | -0.047 | -0.087 | -0.029 | -0.026 | -0.036 | -0.038 | -0.018 |
| **AVERAGE** | **0.194** | **0.195** | **0.166** | **0.167** | **0.158** | **0.160** | **0.107** | **0.109** | **0.116** | **0.119** |
| | | | | | | | | | | |
| **RS-X** | 0.127 | 0.038 | 0.127 | 0.038 | 0.127 | 0.038 | 0.105 | 0.031 | 0.105 | 0.031 |
| **RS-Y** | 0.038 | 0.127 | 0.038 | 0.127 | 0.038 | 0.127 | 0.031 | 0.105 | 0.031 | 0.105 |

# 9 APPENDIX C

In Figures 14-??, force deformation hysteretic behaviors of three different isolators, locations shown in Figure14, are given for earthquake Hector1787 (#3) with MCE lower bound parameters. Axial force history of three isolators are also provided in Figure ??a and ??b. Selected isolator Iso 1 is under a stable compression behavior and located relatively inside the structure when compared to other isolators. Iso2 is located at one of the edges, and exhibits no tensile forces, but highly varying axial load in compression. Finally, Iso 3 is located at a corner and show varying axial load behavior between tension and compression. Since they are located at the sides of the structure Iso 2 and Iso 3 are subjected to relatively higher rotational movements than Iso 1.

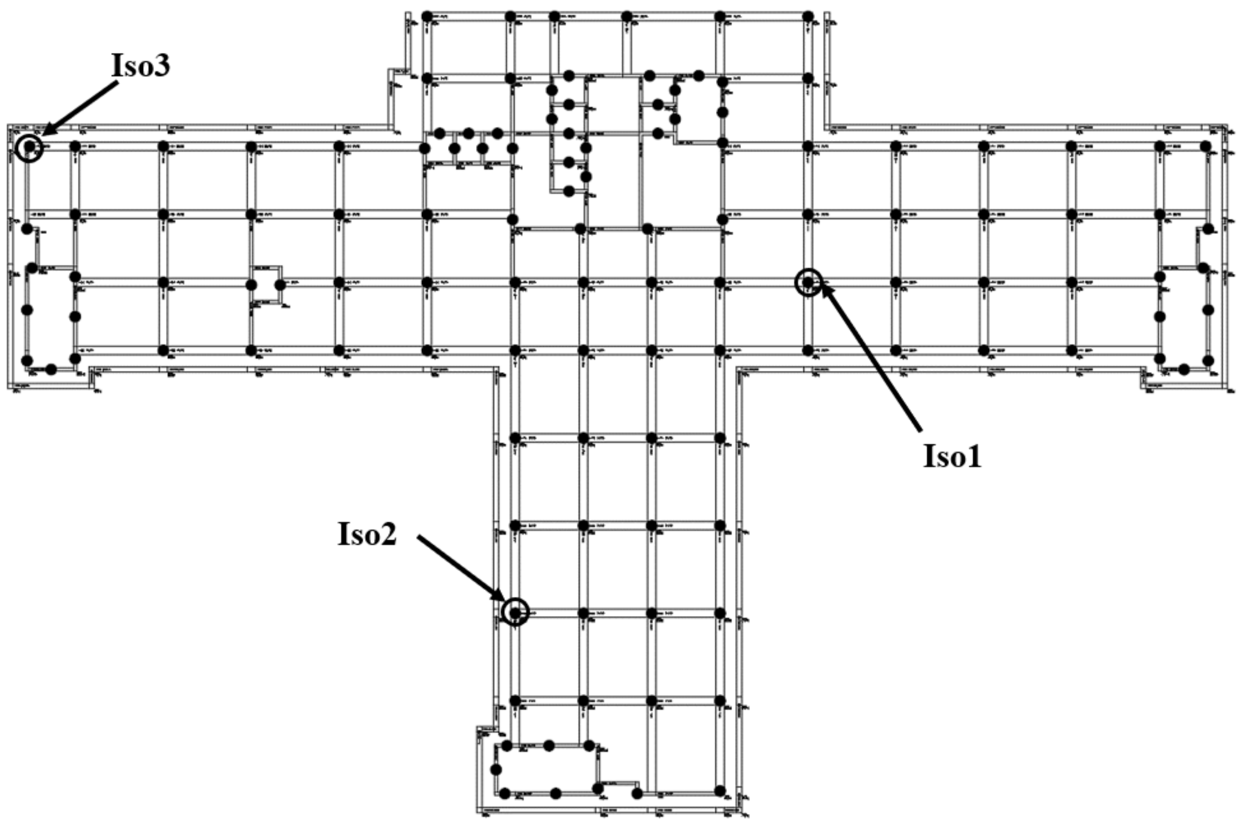


Figure 13. Selected isolators in order to show hysteretic curves

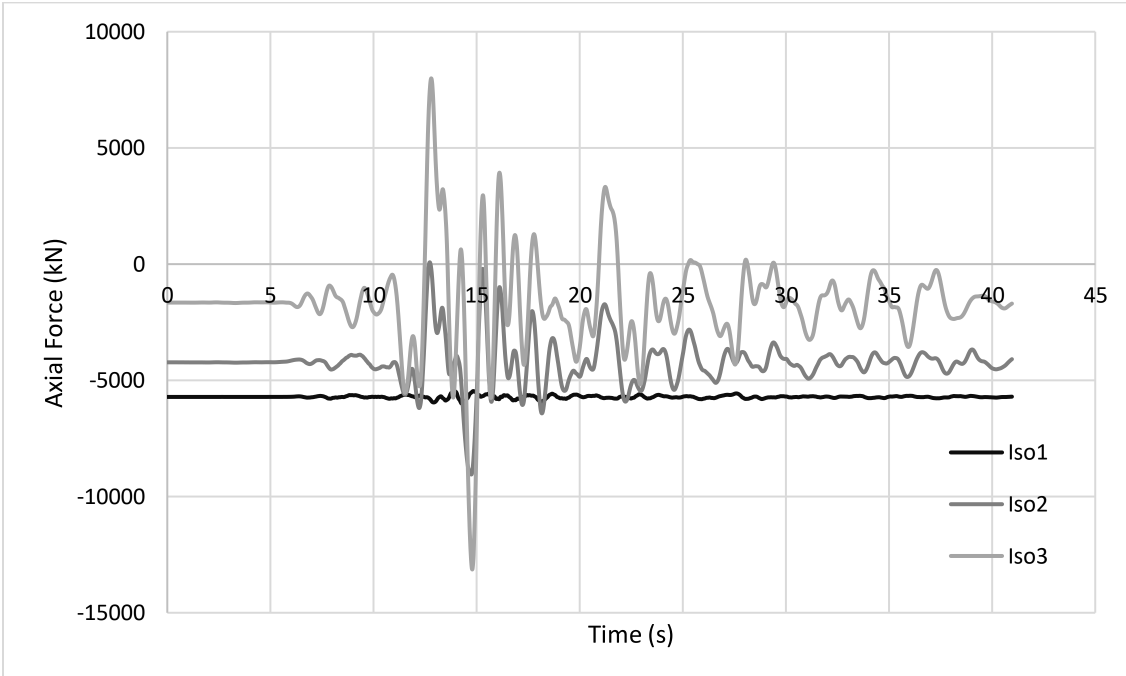


Figure 14a. Axial force history of three isolators with HDRB-DHI model under Kobe1116 (#4) ground motion

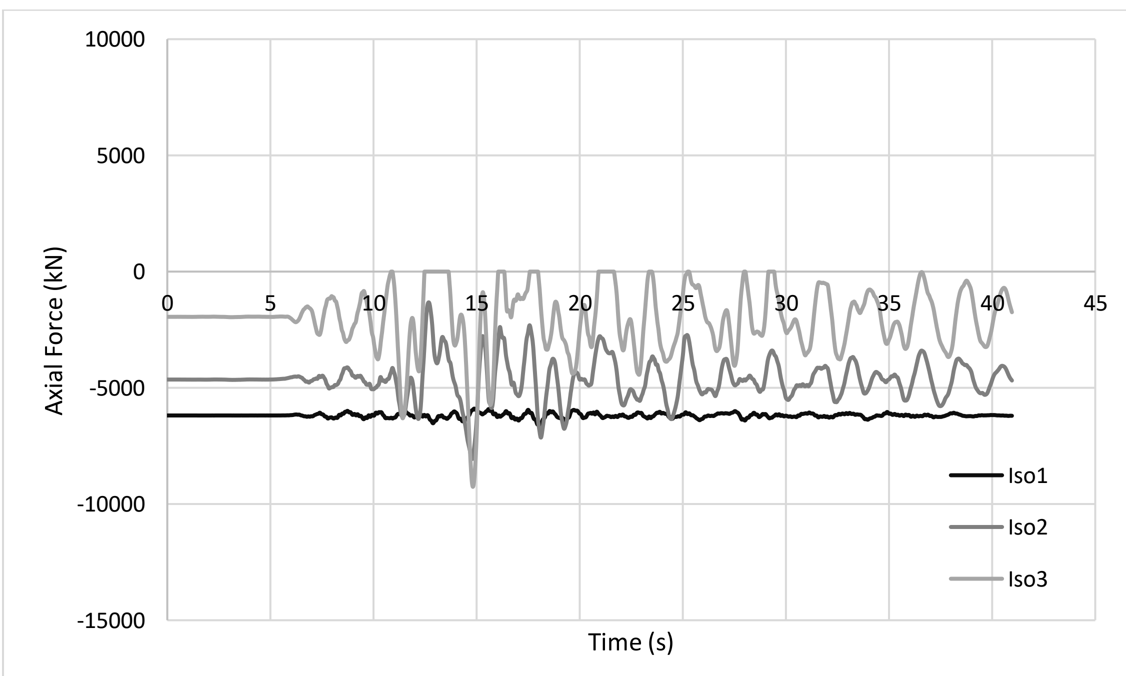


Figure 15b. Axial force history of three isolators with HDRB-DHI model under Kobe1116 (#4) ground motion

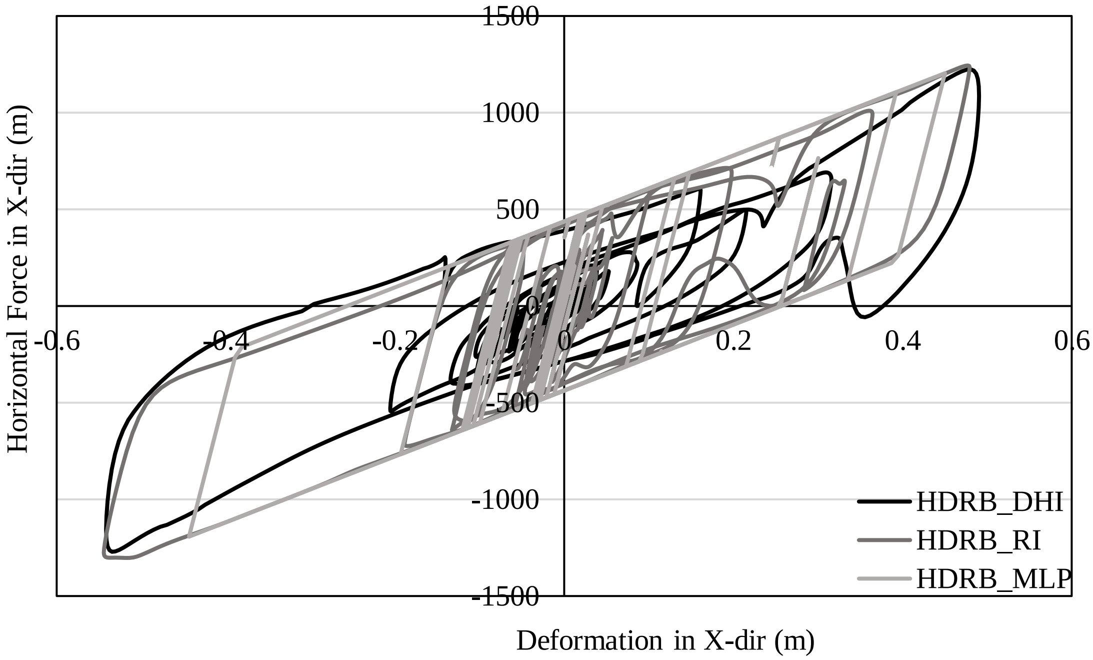


Figure 16. Hysteresis curves of Iso1 under Kobe1116 (#4) for HDRB isolators in X direction

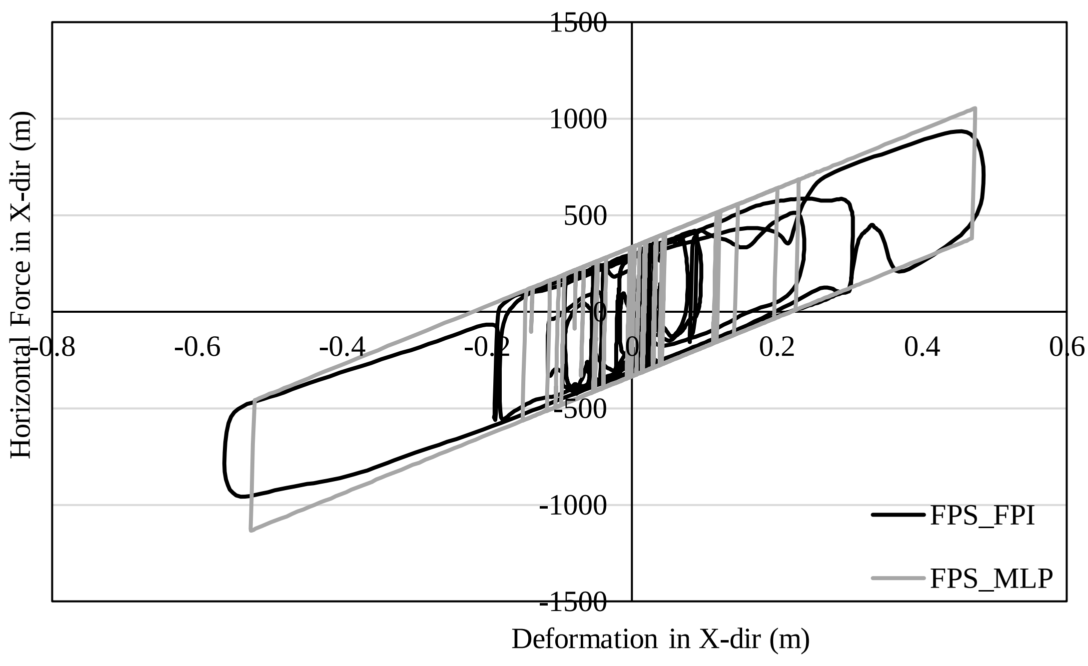


Figure 17. Hysteresis curves of Iso1 under Kobe1116 (#4) for FPS isolators in X direction

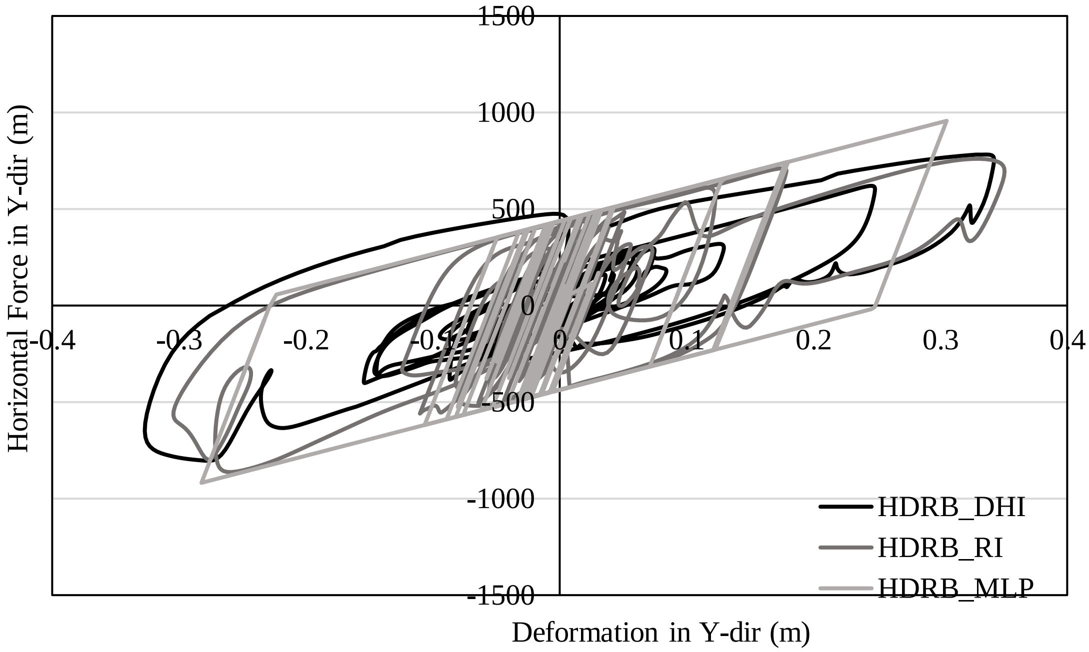


Figure 18. Hysteresis curves of Iso1 under Kobe1116 (#4) for HDRB isolators in Y direction

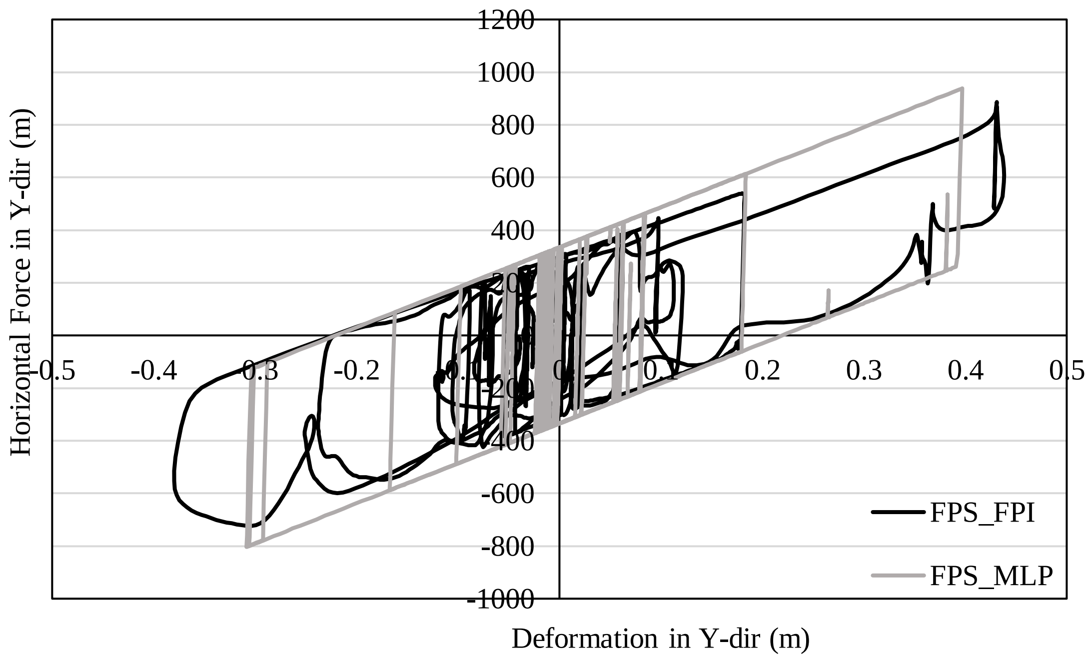


Figure 19. Hysteresis curves of Iso1 under Kobe1116 (#4) for FPS isolators in Y direction

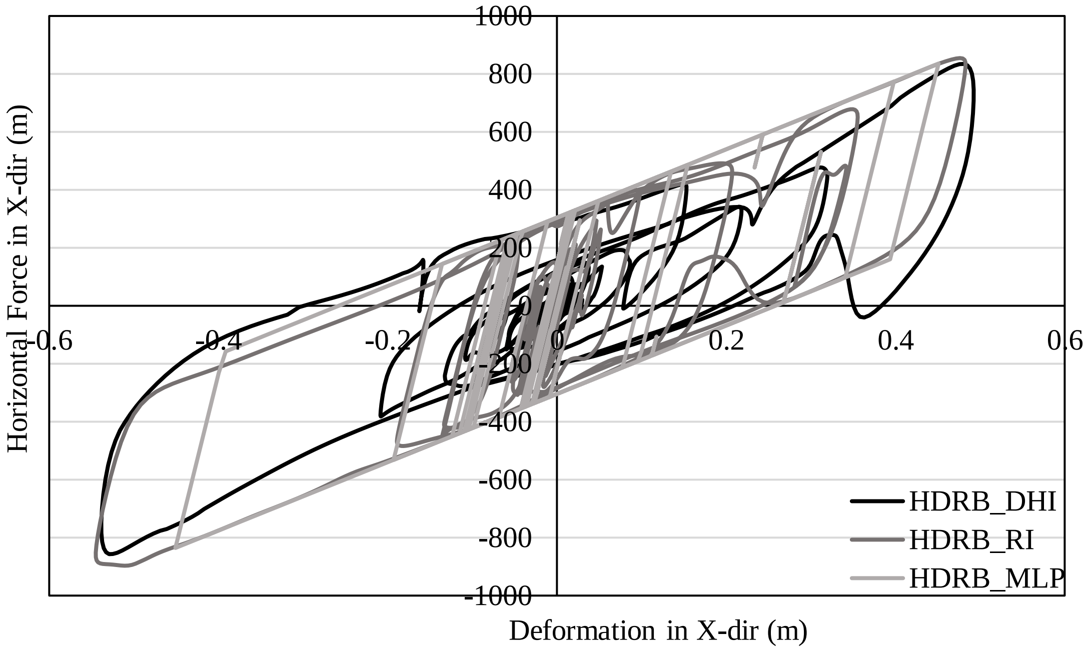


Figure 20. Hysteresis curves of Iso2 under Kobe1116 (#4) for HDRB isolators in X direction

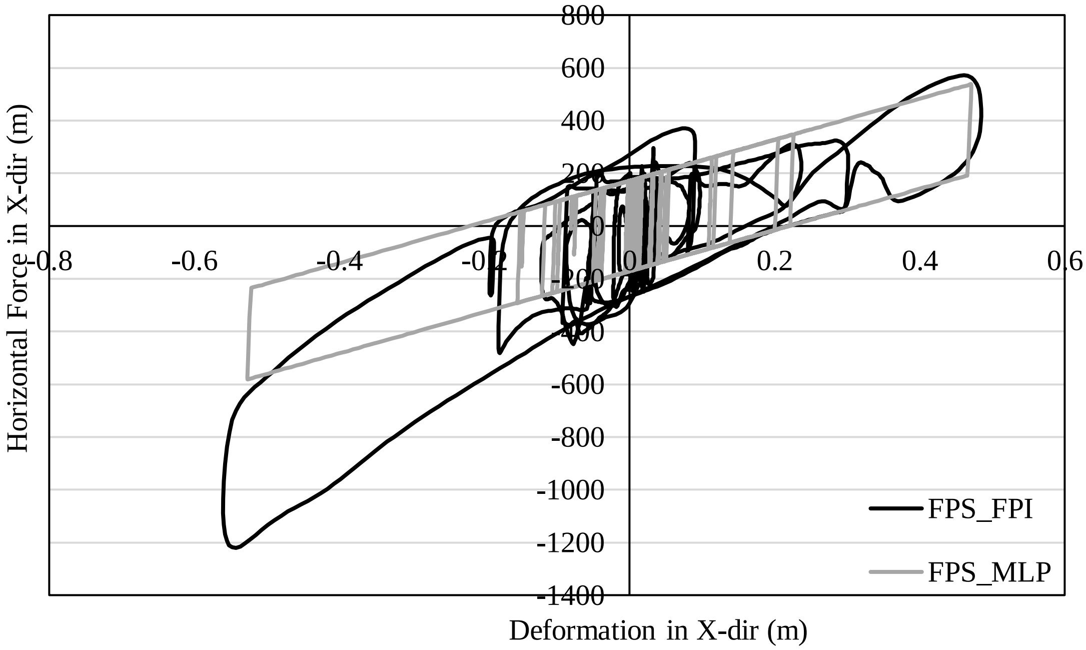


Figure 21. Hysteresis curves of Iso2 under Kobe1116 (#4) for FPS isolators in X direction

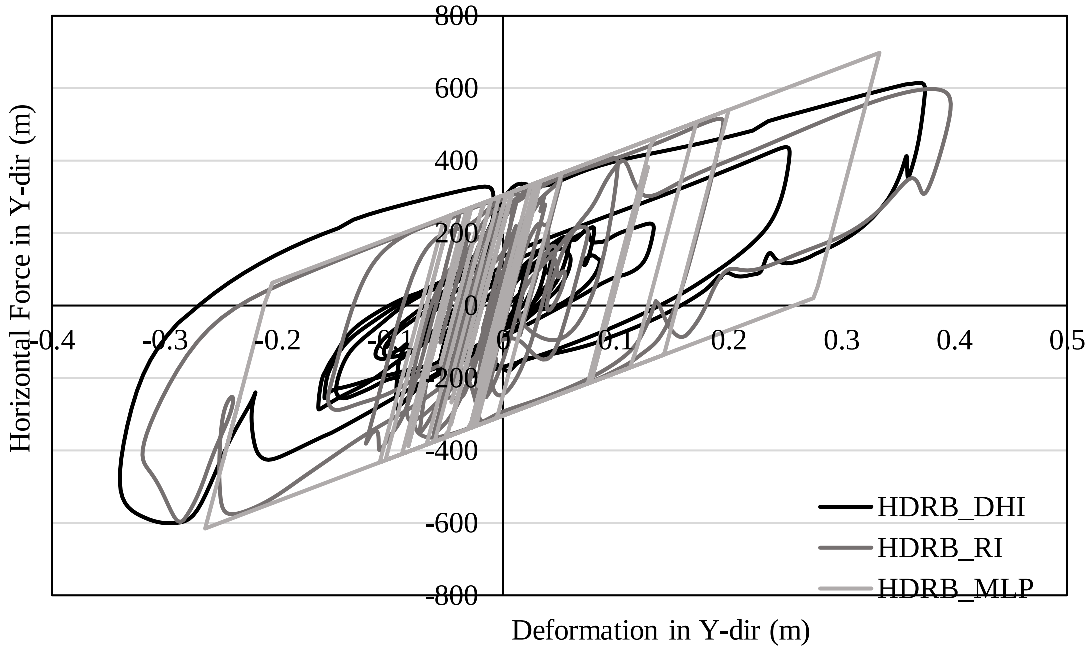


Figure 22. Hysteresis curves of Iso2 under Kobe1116 (#4) for HDRB isolators in Y direction

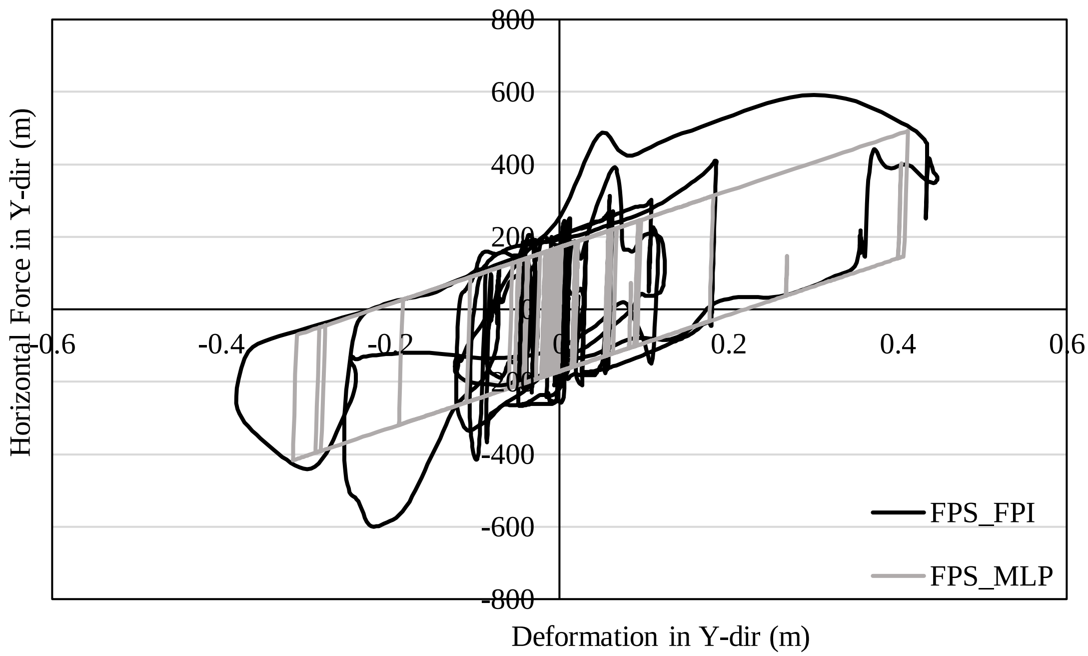


Figure 23. Hysteresis curves of Iso2 under Kobe1116 (#4) for FPS isolators in Y direction

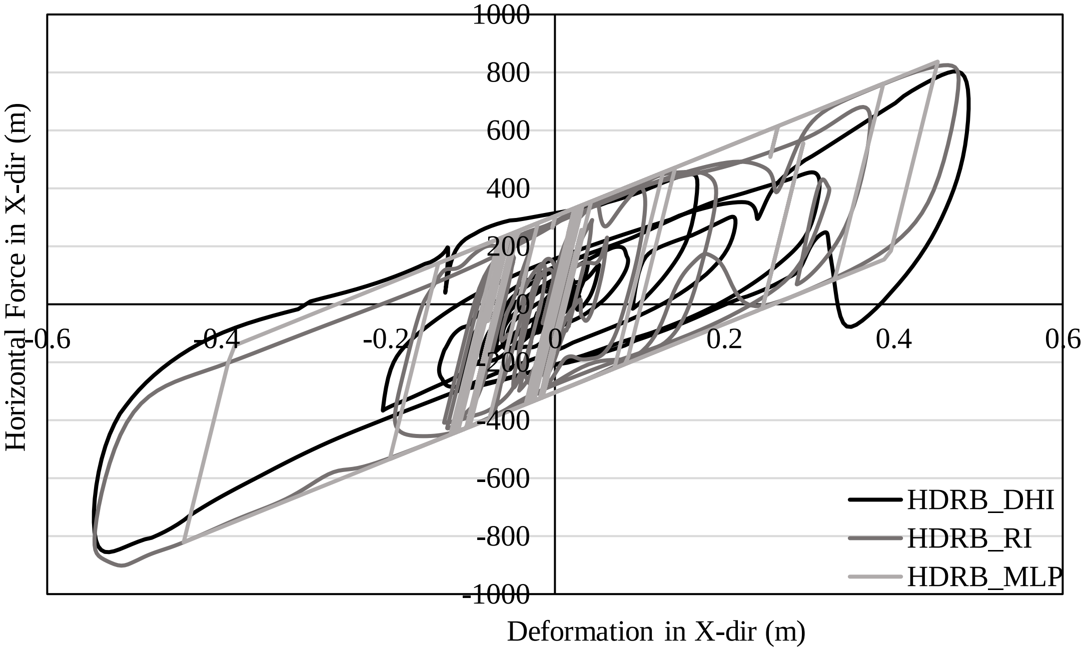


Figure 24. Hysteresis curves of Iso3 under Kobe1116 (#4) for HDRB isolators in X direction

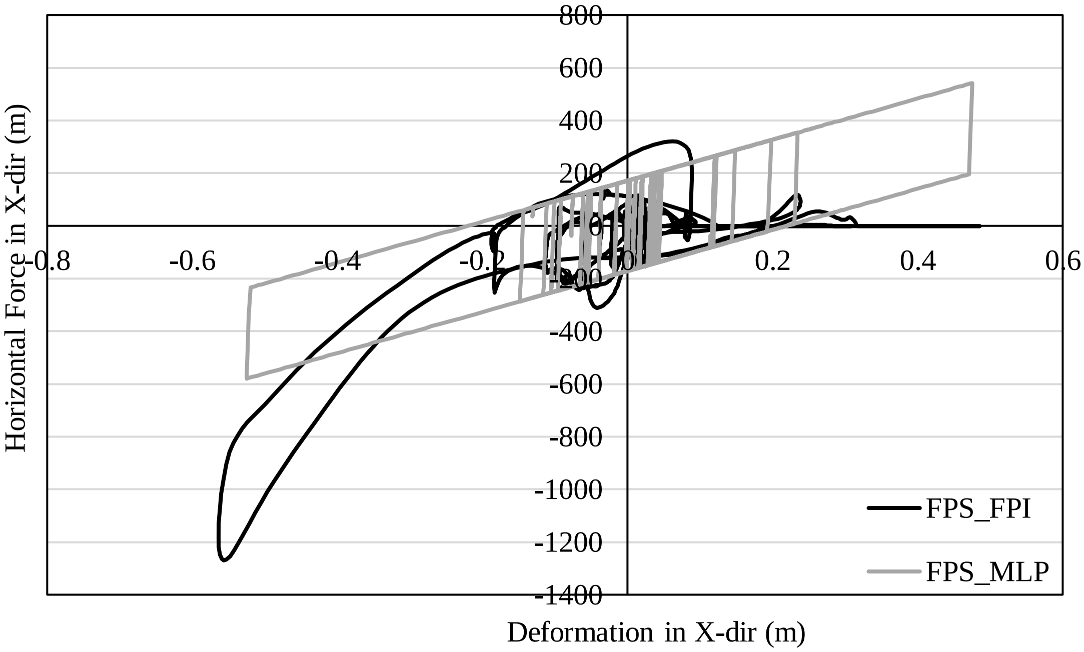


Figure 25. Hysteresis curves of Iso3 under Kobe1116 (#4) for FPS isolators in X direction

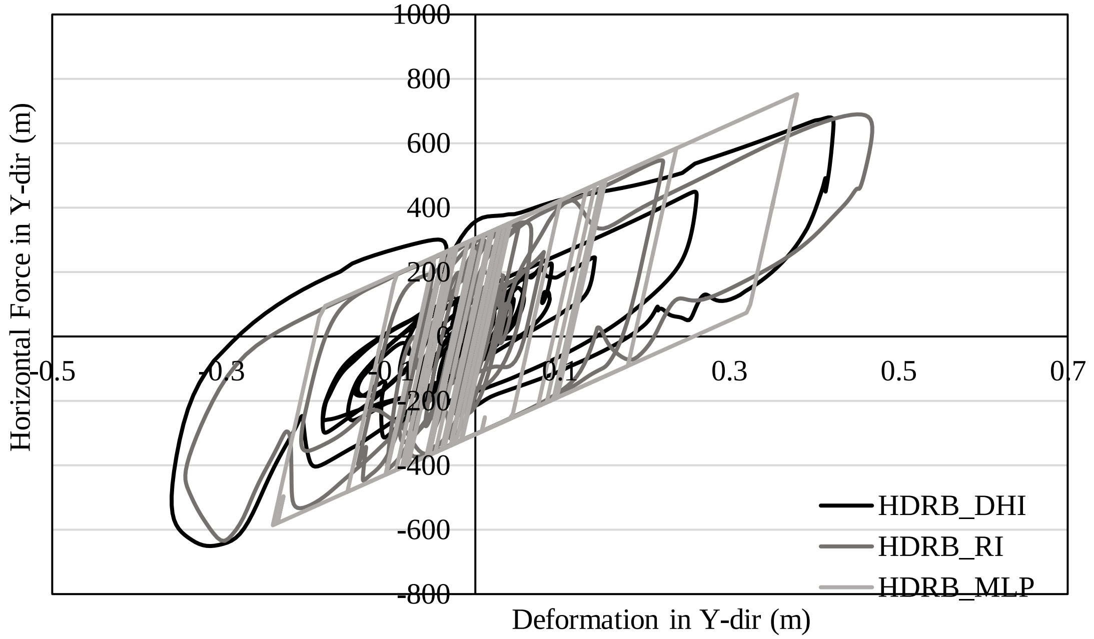


Figure 26. Hysteresis curves of Iso3 under Kobe1116 (#4) for HDRB isolators in Y direction

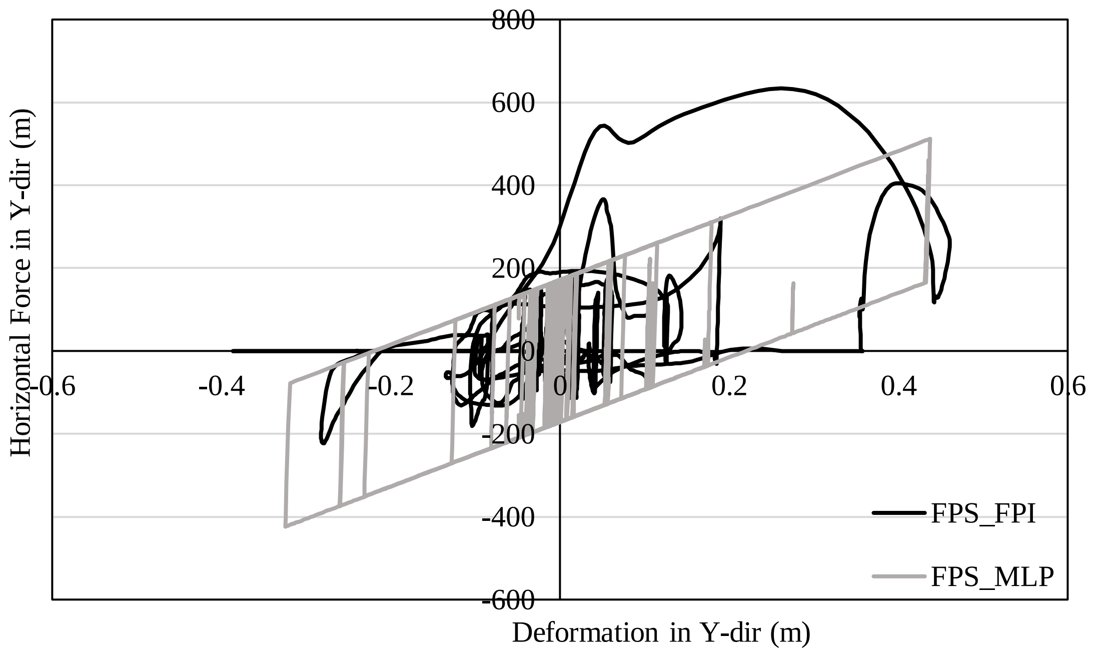


Figure 27. Hysteresis curves of Iso3 under Kobe1116 (#4) for FPS isolators in Y direction